Insights from CMIP6 for Australia's future climate

Grose MR[1], Narsey S[2], Delage FP[2], Dowdy AJ[2], Bador M[3], Boschat G[2], Chung C[2], Kajtar J[4], Rauniyar S[2], Freund MB[5], Lyu K[1], Rashid H[6], Zhang X[1], Wales S[3], Trenham C[7], Holbrook N[4], Cowan T[8], Alexander L[3], Arblaster JM[9], Power S[2]

1. CSIRO Oceans and Atmosphere, Hobart Australia
2. Australian Bureau of Meteorology, Melbourne Australia
3. University of New South Wales, Sydney Australia
4. Institute of Marine and Antarctic Studies, University of Tasmania Hobart Australia
5. CSIRO Agriculture and Food, Hobart Australia
6. CSIRO Oceans and Atmosphere, Melbourne Australia
7. CSIRO Oceans and Atmosphere, Canberra Australia
8. University of South Queensland, Toowoomba Australia
9. ARC Centre of Excellence for Climate Extremes, Monash University, Melbourne Australia

Abstract

Outputs from new state-of-the-art climate models under the Coupled Model Inter-comparison Project phase 6 (CMIP6) promise improvement and enhancement of climate change projections information for Australia. Here we focus on three key aspects of CMIP6: what is new in these models, how the available CMIP6 models evaluate compared to CMIP5, and their projections of the future Australian climate compared to CMIP5 focussing on the highest emissions scenario. The CMIP6 ensemble has several new features of relevance to policy-makers and others, for example the integrated matrix of socio-economic and concentration pathways. The CMIP6 models show incremental improvements in the simulation of the climate in the Australian region, including a reduced equatorial Pacific cold-tongue bias, slightly improved rainfall teleconnections with regional climate drivers, improved representation of atmosphere and ocean extreme heat events, as well as dynamic sea level. However, important regional biases remain, evident in the excessive precipitation over the Maritime Continent and precipitation pattern biases in the nearby tropical convergence zones. Projections of temperature and rainfall from the available CMIP6 ensemble broadly agree with those from CMIP5, except for a group of CMIP6 models with higher climate sensitivity and greater warming and increase in some extremes after 2050. CMIP6 rainfall projections are similar to CMIP5, but the ensemble examined has a narrower range of rainfall change in summer in the north and winter in the south. Overall, future national projections are likely to be similar to previous versions but perhaps with some areas of improved confidence and clarity.

1. Introduction

The new Coupled Model Inter-comparison Project phase 6 (CMIP6) multi-model ensemble (Eyring et al. 2016) builds upon the previous phase 5 (Taylor et al. 2012) and enables new opportunities to examine the climate system and make regional projections of the climate under future scenarios, including for Australia. CMIP6 includes coupled atmosphere-ocean general circulation model (AOGCM) and Earth system model (ESM) simulations of the global climate, taken together under the umbrella term global climate model (GCM). Previous CMIP ensembles have been used as inputs to the Intergovernmental Panel on Climate Change (IPCC) fourth and fifth assessment reports, AR5 and AR6 (IPCC 2007; IPCC 2013) and as the main inputs to Australian national climate projections projects, complemented by dynamical and statistical downscaling (CSIRO and Bureau of Meteorology 2007; CSIRO and Bureau of Meteorology 2015). The new CMIP6 ensemble will be of strong interest for both assessing climate change processes as part of the sixth IPCC assessment report, and for producing updated national climate change projections for Australia, as well as providing new insights into the climate system and climate change relevant to the region.

CMIP6 will provide value for producing national climate projections products for Australia in three main areas. Firstly, CMIP6 projections are run under a new framework of socio-economic as well as emissions pathways, with some models including climate processes and earth system elements that were not included in previous generations. Secondly, any improvement in the evaluation of these models against the observed climate may lead to increased confidence in certain climate projections. Thirdly, any different future projections in CMIP6 compared to CMIP5 are of strong interest for the world, and for Australia. This includes cases where there is increased model agreement of constrained projected ranges of projected change, or conversely where projected changes from CMIP6 are outside the CMIP5 range for a given forcing scenario.

One important new attribute of CMIP6 is the presence of a group of models with higher climate sensitivity than were in CMIP5 (NCC Editorial 2019). The equilibrium climate sensitivity (ECS), also referred to as effective climate sensitivity, is defined as the estimated equilibrium global mean surface temperature change for a doubling of CO_2 and calculated from abrupt 4xCO2 simulations using the Gregory et al. (2004) method. Various lines of evidence were used in the IPCC AR5 to estimate that ECS is in the *likely* range 1.5 to 4.5 °C with a <5% chance of being 6 °C or more, and this range has been fairly consistent for over 25 years (Collins et al. 2013, Meehl et al. 2019). The CMIP5 models, one line of evidence incorporated into the IPCC assessed range, had ECS in the range 2.6 to 4.6 °C, whereas CMIP6 contains numerous models with an ECS over 4.6 °C (Voosen et al. 2019). High sensitivity is expected to produce hotter temperature projections and greater changes in temperature extremes as well as some other climate variables for the globe and for Australia for a given scenario. The cause of the higher ECS is currently under investigation, but analysis of a few models suggests that stronger cloud feedbacks are one key factor (Gettelman et al. 2019; Forster et al 2019). Currently the ECS can't be reliably constrained by observed trends (Gregory et al. 2019), and high values can't be ruled out. Therefore, we don't make any decision whether the ECS values are implausible to reject models on this basis, but rather we present all available results. Also of note is that a number of models (e.g. Sellar et al. 2019) have stronger than observed cooling during the period of strong aerosol forcing (1950s-1970s).

Here we examine the available CMIP6 ensemble as it relates to producing climate projections for Australia. This study includes a discussion of the three aspects above: what is new in the models (discussed in the Data and Methods section), how CMIP6 models evaluate compared to previous generations, and the CMIP6 projections of the future climate. The CMIP6 ensemble does not contain a full set of models yet, and may not do so for months or years, so the model results considered here are not a full ensemble. Instead we present available CMIP6 simulations against the range of CMIP5 simulations, to see if the new models show any systematic improvements or provide projections that are outside of the CMIP5 range.

2. Data and Methods

2a. New features of the CMIP6 database relevant to Australian climate projections

The main focus of this paper is on the new simulations of the future climate under scenarios of human emissions, referred to as ScenarioMIP (O'Neill et al. 2016). There are important new developments in ScenarioMIP compared to CMIP5, but there are also features of the other MIPs that are relevant as well.

Simulations in CMIP5 were made under a set of scenarios of anthropogenic greenhouse gas and aerosol concentrations resulting in different levels of radiative forcing – the Representative Concentration Pathways (RCPs) outlined in van Vuuren et al. (2011). Each ScenarioMIP simulation in CMIP6 is made under a combination of an RCP and a Shared Socio-economic Pathway (SSP), outlined in Meinshausen et al. (2019), named for the SSP value then the RCP value. The RCPs, defined by the magnitude of enhanced radiative forcing at 2100 contain the same values as for CMIP5 but include some new ones: 1.9, 2.6, 3.4, 4.5, 6.0, 7.0 and 8.5 W m^{-2}. The five SSPs are summarised by the narrative headlines; SSP1 – Sustainability: taking the green road; SSP2 – Middle of the road; SSP3 – Regional rivalry: a rocky road; SSP4 – Inequality: a road divided; and SSP5 – Fossil-fuelled development: taking the highway. At the time of writing, and possibly for some time to come, outputs are only available for the 'Tier 1' combinations: SSP1-26, SSP2-45, SSP3-70 and SSP5-85.

The framing by both SSP and RCP dimensions provides new opportunities to examine the future in terms of physical climate change and global socio-economic pathways, including the interactions between the two.

There are also important new developments in other MIPs that are relevant to understanding climate and climate change in Australia and producing projections, that are not discussed in this paper. These include: Decadal prediction (DCPP), high spatial resolution simulations (HighResMIP), Coordinated regional downscaling experiment (CORDEX), vulnerability, impacts, adaptation and climate services advisory board (VIACS AB), Geoengineering (GeoMIP), Detection and attribution (DAMIP) and Paleoclimate simulations (PMIP). In the fullness of time the outputs of these MIPs, and the insights derived from them, will be of potential interest and value in understanding climate processes in Australia and producing national climate projections for Australia.

2b. Methods

This study uses one simulation each from up to 32 CMIP6 models that are available at the time of writing (Table 1), with most models having Historical simulations available for evaluation purposes and fewer models available for ScenarioMIP. The focus for projections is on the SSP5-85 experiments, as this provides the strongest climate change signal, where typically 16 models were examined (more for mean annual temperature, fewer for extremes analyses, not all models are available for all analyses). We compare this to up to 32 CMIP5 models for Historical and RCP8.5 simulations.

For producing spatial analyses model outputs were regridded to a common 1.5 x 1.5 °lat/lon regular grid. Evaluation was conducted in 1950-1999 or 1950-2005 (as marked) for ocean, driver, and teleconnection analyses, and for the IPCC AR6 baseline 1995-2014 for temperature and rainfall. Observed datasets used are Australian Water Availability Project (AWAP) temperature and rainfall for Australia (Raupach et al. 2009), HadISST1.1 for SST (Rayner et al. 2003), and GPCP for Indo-Pacific rainfall (Adler et al. 2003).

Mean Climate

One means of evaluating climate models is to compare their simulation of the historical climate against observations (e.g. Flato et al. 2013). Doing so enables us to identify particular regions and processes where models may be in some way deficient (e.g. Christensen et al. 2013). This information may then be used to inform the confidence in the relevant climate change projections provided by these models. We evaluate the climatological mean state of the historical simulation of precipitation and SST, comparing the performance of a subset of CMIP5 and CMIP6 models for two seasons: June to November (JJASON), and December to May (DJFMAM). We focus this analysis on the region surrounding the Australian

continent, including the two major ocean basins relevant to several large-scale circulations and climate drivers which influence the Australian climate (e.g. Risbey et al. 2009).

A common and long-standing mean-state bias in CMIP models over the years has been the "cold tongue bias", which is the penetration of the equatorial Pacific cold tongue too far west (Mechoso et al. 1995; Li and Xie 2014). This bias plays an important role in the simulation of current and future climate in the tropical Pacific and surrounding regions. For example, studies of CMIP5 models have shown that this bias can lead to a cold sea surface temperature (SST) bias in the western Pacific which would contribute to a La Niña-like response to increasing Greenhouse gases (Li et al. 2016; Ying et al. 2019). It also contributes to biases in the simulation of ENSO and related teleconnections, leading to weakened Australian monsoon westerlies (Colman et al. 2011) as well as limited skill in the seasonal prediction of the Asian summer monsoon (Li et al. 2019). This bias affects the projections of regional rainfall in the western Pacific (e.g. Grose et al. 2014) and also the northern Australian monsoon region (e.g. Brown et al. 2016).

Two methods are employed to evaluate the Pacific cold tongue bias adjacent to Australia. The first method is to use the eastern edge of the Indo-Pacific warm pool as a marker, defined as the equatorial longitude of the 28.5°C isotherm (Brown et al 2013; Grose et al 2014). In observations, this represents the boundary between the warm, fresh water of the warm pool and colder, saltier water of the cold tongue (Brown et al. 2013b; Grose et al. 2014) and is located at 186.5 °E during the late historical period (JJASON, 1950-2005). This method, while useful, does have some drawbacks. In particular, the 28.5°C isotherm being the edge of the warm pool is true in observations, but this value may differ by up to 1° longitude in models (Brown et al 2015). An alternative method is to introduce a cold tongue index (CTI), defined to be the bias in the SSTs averaged over the warm pool (155 °E to 175 °E, 10 °S to 10 °N). In this way, any extension of the models' cold tongue into the observed warm pool region would result in CTI < 0.

Extremes

Extremes indices defined by the Expert Team on Climate Change Detection and Indices (ETCCDI) in Zhang et al. (2011) were calculated from daily precipitation and daily minimum and maximum temperatures using the Climpactv2 software (https://climpact-sci.org/get-started/) for both AWAP and models. These indices describe different aspects of precipitation and temperature extremes. We choose 6 of the possible 27 ETCCDI indices in order to measure aspects of intensity, frequency and duration:

- TXx: annual maximum value of daily maximum temperature (^{o}C) (intensity)
- TNn: annual minimum value of daily minimum temperature (^{o}C) (intensity)
- wsdi (warm spell duration index): annual count of days with at least 6 consecutive days when daily maximum temperature> 90th percentile (duration)
- Rx1day: annual maximum value of daily precipitation (mm) (intensity)
- R10mm: annual count of days when precipitation ≥ 10mm (days) (frequency)
- CDD (maximum length of dry spell): maximum number of consecutive dry days (i.e. with precipitation < 1mm) (days) (duration)

Fewer CMIP6 model outputs are available at the daily compared to the monthly scale, so only seven CMIP6 models were available to be analysed (Tabel 1). Indices were calculated on the native grids of the observations and models before being interpolated onto the 1.5 x 1.5 ° lat/lon regular grid. Climatological values of the indices from 1995 to 2014 from AWAP are shown in Supp. Figure 1.

Average recurrence intervals (ARI) were also calculated from daily data. This was done for 1-, 5- and 10-year ARI values, for precipitation and tasmax. The ARI values were calculated for the period 1950 to 1999, as well as for the period 2050-2099, enabling the projected change in ARI to be examined. While noting that there are various methods that can be used for calculating ARI values, the method used here is based on ranking the days in order of magnitude and then finding the day corresponding to the given ARI (i.e., the 5th highest daily value in the 50 year period is used for estimating the 10-year ARI, while the 50th highest value is used to estimate the 1-year ARI).

ENSO, IOD and SAM

Special focus is given here to the simulation of the ENSO, IOD and SAM and their teleconnection to Australian rainfall, since these phenomena are important to Australian rainfall variability and may be important to future changes in the climate.

The El Niño-Southern Oscillation (ENSO) and Indian Ocean Dipole (IOD) exhibit teleconnections to Winter-Spring rainfall (JJASON) in Australia. ENSO variability is tracked using the DJF NINO3.4 index (Bellenger et al. 2014), while the SON Dipole Mode Index (DMI; Meyers et al. 2007; Liu et al. 2014) is used for the IOD. Both indices had their seasonal cycles removed and the resulting anomaly timeseries were detrended using a cubic polynomial fit. While the IOD is known to co-vary with ENSO (and vice-versa), with the strongest impacts on rainfall over eastern Australia (Meyers et al. 2007; Risbey et al. 2009; Cai et al. 2011), in this simple analysis, we do not separate the impacts of ENSO from the IOD.

The Southern Annular Mode (SAM) is the leading mode of atmospheric variability in the Southern Hemisphere and has also been shown to affect rainfall variability in Australia. A positive phase of SAM refers to a poleward shift of the eddy-driven jet, resulting in increased rainfall over high latitudes and decreased rainfall over midlatitudes in all seasons, and also higher rainfall over the subtropics in austral spring-autumn (Thompson and Wallace, 2000; Hendon et al. 2007, 2014a; Lim et al. 2016). We calculate the monthly SAM index following the definition of Gong and Wang (1999), as the difference in zonal mean sea level pressure (MSLP) anomalies between 40°S and 65°S in each CMIP model and compared with the observed SAM calculated from ERA-Interim reanalyses (Dee et al, 2011). The 1979-2005 time period is used for normalisation in each case.

Additionally, ENSO phase-locking was examined in 1870-2014 in thirteen CMIP6 models and 18 CMIP5 models for which SST data are available for both the Historical and SSP585/RCP8.5 experiments for the full period, and in HadISST. The Niño-3.4 index was calculated first by averaging full SSTs over the Niño-3.4 region (190 °E to 240 °E, 5 °S to 5 °N). The model Niño-3.4 indices show pronounced long-term nonlinear trend, akin to global warming signal. This nonlinear trend was estimated and removed by fitting a 3rd-order polynomial function to the combined Historical and SST585/RCP8.5 Niño-3.4 index.

The zonal structure of ENSO related SST variability was evaluated using the standard deviation along the tropical equatorial Pacific (zonal average 2 °S to 2 °N) in observations (HadISST, 1870-2014) and CMIP simulations. All available historical experiments included 32 CMIP5 models and 28 CMIP6 models during the full period. An ensemble comparison of the historical experiments with available SSP585/RCP8.5 experiments was conducted based on a subset of 31 CMIP5 and 19 CMIP6 models for which both experiments were available.

Marine Heatwaves

Marine heatwaves (MHWs) are periods of anomalously warm ocean temperatures, which can span several days to months (Hobday et al. 2016). In extreme cases, MHWs can have significant impacts on marine ecosystems, leading to loss of species and habitats (Smale et al. 2019). The frequency, duration, and intensity of MHWs have increased over the past century across the globe, and Australia's marine environment is no exception (Oliver et al. 2018). Marine ecosystems are of vital importance to Australia's fisheries, aquaculture, tourism, and identity (Holbrook and Johnson 2014; Johnson and Holbrook 2014), and thus the more extreme MHWs projected under climate change pose a significant risk. The representation of MHW intensities and durations in the historical period are evaluated in this paper.

Marine heatwave (MHW) annual statistics were calculated from SST during 1982-2014 in CMIP6 and CMIP5 models (using Historical and RCP4.5 simulations to match CMIP6) on a grid point basis and compared to the 0.25 °lat/lon NOAA OI SST V2 product (Reynolds et al. 2007). Outputs were examined on native grids then nearest neighbour interpolation was used to present data on the observed grid. MHW events were examined as events of SST over the 90th percentile of temperature on that calendar day (using an 11-day window centred on the given day in the 1996-2014 baseline in each model) for at least five consecutive days. MHW periods separated by less than three days are considered a single event. After computing the threshold for each calendar day, it was smoothed by applying a 31-day moving

mean. The intensity of MHWs is thus taken as the maximum temperature anomaly of the event, relative to the climatological mean.

Sea level

In this study, we only consider the dynamic sea level (DSL) change simulated by the climate models, which does not include the other sea level components related to melting of land ice, i.e. the glaciers and polar ice sheets. The DSL is closely related to ocean density and circulation thus its regional distribution can be explained well by ocean dynamics. Dynamic sea level change determines the regional pattern of change in sea level experienced at the coast. Observations and previous modelling suggest that there is considerable variation in dynamic sea level change around Australia in the past and the projected future, with higher rates of change in the north and east and lower rates on the south coast. Downscaling of CMIP5 sea level projections suggests these regional patterns could be enhanced compared to the global simulations (Zhang et al. 2017). Here we evaluate CMIP6 simulation of dynamic sea level and examine the projected change with a comparison to previous downscaled projections. We do not address the other contributions to total sea level change.

We examine the components of sea level that are included in CMIP models, those of thermal expansion, change to ocean currents and changes to land storage. Loss of land ice required for total sea level change analysis is not included here.

3. Evaluation

To inform confidence in future climate projections we first evaluate some of the key features of climate model simulations. The Indian Ocean to the northwest and the Pacific Ocean to the northeast of Australia are both critical to Australian climate variability and change, both in terms of their mean state (e.g. relative temperature of Indian compared to Pacific) and also climate variability through processes including ENSO and IOD. Therefore, the focus here is on the entire Indian-Pacific region rather than just Australia.

3a. Mean climate

The bias in SST is similar between CMIP5 and CMIP6 (Figure 1), but with some cases where the bias is different in magnitude and some new features exist. The cool bias in JJASON in the Tasman Sea, Pacific Ocean, Inter-Tropical Convergence Zone (ITCZ) and the South Pacific Convergence Zone (SPCZ) regions is similar to CMIP5 in extent but slightly lower in magnitude. There is a warm bias in the equatorial Indian Ocean during DJFMAM that was not present in CMIP5.

Most of the CMIP5 models simulate the 28 °C isotherm too far west, with the equatorial isotherm of the multi-model mean (MMM) located at 163.5 °E. In CMIP6, there is a marked reduction of this bias, with the MMM isotherm at 172.5 °E (Figure 2). Figure 2d shows the model spread of the longitude of the 28.5 °C isotherm, with more than 81% of CMIP5 and 93% of CMIP6 models simulating the isotherm too far west. Note that although a larger fraction of CMIP6 models place the equatorial isotherm too far west, the interquartile range is smaller and closer to the observed value. The spread of the CTI in the models can be seen in Figure 2b and quantified in Figure 2e, with the CMIP5 MMM being -0.39 °C and the CMIP6 MMM being –0.12 °C. We find 79% and 67% of CMIP5 and CMIP6 models respectively have a CTI < 0. Both methods presented here show that there is an encouraging improvement in the cold tongue bias in the CMIP6 models. It is expected that this improvement will lead to a reduction in the related biases discussed previously.

Like temperature, the spatial distribution of bias in seasonal precipitation is similar in the two ensembles (Figure 3), including a wet bias in the cold-tongue region and Maritime Continent persisting in CMIP6. A dry bias in the southeast SPCZ region and wet bias in the off-equatorial east Pacific, indicate a continued double-ITCZ, or overly zonal SPCZ bias in CMIP5. This has not changed substantially in CMIP6. The dry bias in the eastern Indian Ocean during JJASON is increased for CMIP6 models surveyed. There is still an overly zonal SPCZ (Brown et al. 2013a). Excessive precipitation biases remain in the Maritime Continent region, which may relate to local Hadley circulation biases (e.g. Toh et al. 2018). One notable improvement is a

decrease in SST bias in the western equatorial Pacific, a region where historical biases were associated with projected drying over northern Australia (Brown et al. 2016). Looking at rainfall in more detail over Australia compared to the gridded AWAP rainfall dataset (Figure 3d, e), we see the mean wet bias in most locations, but with dry biases related to topography and coastlines, as expected from the GCM coarse resolution.

Overall the pattern correlation of precipitation and temperature climatologies is improved in CMIP6 compared to CMIP5. The root mean squared error when comparing model climatologies to observations is lower for the CMIP6 ensemble compared to CMIP5, although the improvement is less pronounced for surface temperature than for precipitation (Figure 4).

3b. Extremes

This evaluation of extremes needs careful interpretation as there are fewer CMIP6 than CMIP5 models (Table 1, 2) meaning the reduction in spread of CMIP6 compared to CMIP5 is at least partly due to a smaller number of models in the ensemble (Supp Figure 2). Bearing this in mind we draw the following conclusions.

For all indices analysed, observed values sit within the spread of both CMIP5 and CMIP6 (Supp. Figure 2) and for TXx, R10mm and CDD observations sit close to the multi-model mean (although not surprisingly have more year to year variability). However, the coldest night of the year is generally cooler in observations than the MMM of either CMIP5 or CMIP6 and there are fewer warm spells. In addition, the wettest day of the year is about 5 to 10 mm more intense in CMIP6 compared to CMIP5 and closer to the AWAP observations. Broadly speaking minimum temperature extremes (e.g. TNn) seem to be warmer and maximum temperature extremes (e.g. TXx) seem to be cooler in CMIP6 compared to CMIP5, at least based on the currently available ensembles. In addition, the spread is much smaller in CMIP6 compared to CMIP5 so there are fewer models with very low or very high values across the majority of indices. One exception is Rx1day where the upper extremes are larger in CMIP6.

Mean biases in the model ensembles compared to AWAP are very similar in terms of spatial pattern and magnitude although in CMIP6 we see some reduction of the bias in TNn and Rx1day over northern and eastern Australia (Supp. Figure 3).

In summary, compared to observations, the results for CMIP5 and CMIP6 are similar for temperature and precipitation extremes although with some indication that CMIP6 has reduced some of the warm bias in TNn and dry bias in Rx1day. This could change as more CMIP6 models become available.

3c. ENSO, IOD and SAM

First we assess the simulation of some important features of ENSO, IOD and SAM then examine the teleconnection of ENSO and IOD to Australian rainfall. Seasonal phase locking of ENSO is similar in CMIP5 and CMIP6 (Supp. Figure 4). In observations the annual maximum and minimum ENSO variability is found in December and June, respectively. The CMIP5 and CMIP6 MMM ENSO variability is similar to observations, with the extreme values occurring in December and June. While the simulated seasonal phase locking is realistic, the ENSO events simulated by the CMIP6 models are stronger than those in observations all year round. The MMM intensity of ENSO events is more realistic in the CMIP5 Historical experiments (dashed blue curve), however, the seasonal phase locking is not as realistic with a smaller annual variation in ENSO variability.

The zonal structure of SST variability represented by the interannual standard deviation is improved in CMIP6 compared to CMIP5 (Supp. Figure 4). In the observations, the strongest interannual variability occurs in the eastern tropical Pacific close to the 100°W longitude. The majority of CMIP5 and CMIP6 models show this peak variability eastwards of 130°W longitude with a few exceptions (CSIRO-Mk3-6-0 & INM-CM4-8). Many of the CMIP5 and CMIP6 models simulate stronger variability than observed, in particular in the central and western Pacific but also in the eastern Pacific. The MMM of CMIP6 historical experiments shows stronger variability compared to CMIP5 models that match the observations more

realistically. However, the location and intensity of simulated interannual variability varies among the models and from the observed and is mostly overestimated in the central and western Pacific.

The observed positive trend in SAM, stronger in summer, in recent decades (1979-2005) is reproduced in the MMM with some bias in the seasonal signature (in particular an underestimation of trends in summer and winter and overestimation in spring) and a large model spread. Results are similar between CMIP5 and CMIP6 (Supp. Figure 5).

The strongest observed correlation of ENSO and rainfall is in eastern Australia (Figure 5a), whereas the strongest correlation with IOD is in southern Australia (Figure 5b). It is notable that the IOD and ENSO teleconnections are remarkably well separated during Winter-Spring over the Australian mainland except for the monsoonal north and the Murray-Darling Basin. Much of the IOD teleconnection with rainfall in the central and western Murray-Darling Basin (and part of the monsoonal north) is due to ENSO (Risbey et al. 2009). ENSO teleconnections to Northern and Eastern Australia tend to be stronger than IOD teleconnections to these regions, while the reverse is true for Southern Australia and the Rangelands.

The ability of CMIP5 and CMIP6 models to simulate ENSO and IOD teleconnections over the NRM super clusters (CSIRO and Bureau of Meteorology 2015) are evaluated in Figure 5. We evaluate ENSO teleconnections to Northern and Eastern Australia (panels C and D) and IOD teleconnections to Southern Australia and the Rangelands (panels E and F). The strength of the ENSO and IOD teleconnection to each region's rainfall is well correlated with the associated amplitude of Niño-3.4 and the DMI. This strong relationship was found in CMIP3 models, although CMIP5 models generate reduced spread in Niño-3.4 and DMI amplitudes than CMIP3 (Cai et al. 2009; Cai and Cowan 2013). The trend towards less diversity in ENSO amplitudes from CMIP3 to CMIP5 (Bellenger et al. 2014) appears to continue from CMIP5 to CMIP6 (horizontal boxplots, Figure 5c-f).

For Northern and Eastern Australia, both CMIP5 and CMIP6 models underestimate the strength of the teleconnection relative to ENSO (vertical boxplots, Figure 5c, d). For Southern Australia and the Rangelands regions which are evaluated for their teleconnection to the IOD, the strength of the teleconnection is still weak but better represented (vertical boxplots, Figure 5e, f). The teleconnection is weak in both CMIP generations despite the fact that the IOD variability is much stronger in models than in observations (horizontal boxplots, Figure 5c, f). The overly strong IOD amplitudes are likely due to model mean state biases with respect to the climatological zonal gradient of the equatorial Indian Ocean thermocline, which in turn generate biases in the mean easterlies and SST gradient (Cai and Cowan 2013).

CMIP6 models show either an improvement or little change in simulating the Winter-Spring rainfall teleconnection to ENSO and IOD over the Australian mainland. While CMIP6 models outperform CMIP5 models in terms of the strength of their ENSO teleconnections to Northern and Eastern Australia, ENSO variability in CMIP6 models is both unrealistically large and larger than that in CMIP5 models. This overestimation of ENSO amplitude does not seem to translate into a stronger IOD amplitude in CMIP6 models as previously found for CMIP5 (Liu et al. 2014), although this may result from having an incomplete set of CMIP6 models.

3d. Marine heatwaves

Modelled MHWs tend to persist longer, are more spatially extensive and less intense than observed events, primarily due to coarse model resolutions (Frölicher et al. 2018). Thus, with higher resolutions in the next generation of climate models (Table 1), there is some hope for improved simulation of mesoscale processes that drive extreme events. In this analysis, we examine whether typical representation of MHWs have improved in CMIP6 relative to CMIP5 (Oliver et al. 2019; their Supplementary Figure 1). We evaluate multi-model mean representations of MHW intensities and durations in SST data. The MHW statistics are computed on native model grids, to avoid smoothing of small-scale features that may occur during re-gridding. Only in the final instance are model results regridded using nearest-neighbour interpolation (see Methods).

The mean of annual maximum MHW intensities are shown for HadISST, CMIP5 MMM and CMIP6 MMM over the period 1982-2014 (Figure 6a-c). MHW intensity is measured as the maximum excursion from the seasonally varying climatology (°C), on a single day in a given year. The day of maximum intensity is further constrained to occur within a MHW event – a period of at least 5 days of extreme warmth (see Methods for further details). The strongest MHW intensities tend to occur off the southeast coast of Australia in observations (Figure 6a). The model means show a similar hotspot (Figure 6b, c), but shifted farther south. The differences between the model means and observed data (Figure 6d, e) show that models generally underestimate MHW intensity, as expected. However, encouragingly, the biases appear to be weaker in the CMIP6 model mean. The time-series of area-average MHW intensities further highlight the typically higher values in CMIP6 as compared with CMIP5 (Figure 6g). One of the CMIP6 models, the *NESM3* model, exhibits significantly larger MHW intensities than any other model or observations. *NESM3* simulates particularly strong variability of SST during the summer season, and thus the anomalous SSTs during MHWs in the summer are large.

The mean number of annual MHW days tends to be overestimated in the model mean, which is also as expected for coarse model simulations (Figure 6h-l). There appears to be a slight improvement on this bias in the CMIP6 model mean (c.f. Figure 6k and Figure 6l), but the improvement is less clear than that in MHW intensity.

This initial assessment suggests CMIP6 simulates MHWs closer to observations than CMIP5, but more models are necessary to determine whether or not the improvement from CMIP5 is significant. Although the MHW intensities look to be much improved, the means of the CMIP5 and CMIP6 model intensities are not significantly different (at the 95% level under a two-sample Student's T-test), nor are the distributions of intensities (at the 95% level under a two-sample Kolmogorov-Smirnov test). There is also no statistically significant correlation between grid resolution and the MHW statistics.

3e. Dynamic sea level

The observed mean sea level over 1992-2012 (Maximenko et al. 2009) shows the effect of ocean currents, as the upper ocean circulation approximately follows contours of constant sea level. For example, the subtropical ocean gyre can be easily recognized in the mid-latitude South Pacific Ocean, with sharper sea level gradient near the East Coast of Australia in the Eastern Australian Current (EAC) region than in the interior of South Pacific. Compared with the observations, both the CMIP5 and CMIP6 ensembles show considerable mean sea level biases around Australia which have been slightly reduced from CMIP5 to CMIP6, as indicated by a smaller root-mean-squared (RMS) error between CMIP5/6 ensemble and observations (5.2 cm for CMIP5 and 4.3 cm for CMIP6) over the region closely surrounding Australia (105 to 150 °E, 0 to 45 °S, Figure 15). The relatively low (high) sea level biases in the western (eastern) tropical Pacific exist in both CMIP5 and CMIP6. Such bias pattern could be explained by the weaker simulated trade winds in the central Tropical Pacific relative to the observations (Lee et al. 2013) and may be closely related to the cold-tongue biases seen in the SST field (Figure 7) .

4. Projections

4a. Mean annual temperature

Under SSP5-85 we see that the upper range of CMIP6 projections by 2100 is hotter than CMIP5 under RCP8.5 for Australia and for the globe (Figure 8a). The value of projected temperature change between the AR6 baseline 1995-2014 and the end of century period 2080-2099 in CMIP6 (Table 1, panels to the right Figure 8a) includes a group of models with a temperature projection higher than any CMIP5 model with values above 5.5 °C Australia. As more models are added, the apparent gap between this group of models and the rest may be filled.

Using the methods of Schurer et al. (2017) to account for warming from pre-industrial to the AR5 baseline, we see that these warmer projections suggest that the global warming target of 2 °C since the pre-industrial era specified in the Paris agreement is likely to be met sooner using the CMIP6 ensemble as

a guide (Figure 8b). As more models are added the CMIP6 curve will change slightly, but the earliest crossing from the hottest models will certainly remain.

Australian warming for the 2080-2099 under SSP585/RCP8.5 is less enhanced relative to global warming in the current CMIP6 models than in CMIP5 (Figure 8c), with no model producing a ratio greater than 1.1, whereas CMIP5 contains 18 out of 35 models with ratios over 1.1 with values up to 1.4. This may be due in part to the greater warming of the Pacific and Northern Hemisphere continents at this timeframe in CMIP6, raising the global value relative to the Australian value (Figure 8d, e). The basic patterns of warming remain, such as enhanced warming over the Arctic, greater warming over land than ocean, delayed warming in the Southern Ocean and the north Atlantic; however the relative magnitude of these are different in the two ensembles. While the temperature projection is generally higher, the projected change in the north Atlantic and Southern Ocean are lower than in CMIP5, suggesting larger ocean heat uptake and that the slowdown in Atlantic meridional overturning circulation (AMOC) is in fact stronger (Supp. Figure 6).

The higher projection for Australia is expected from the higher ECS values in some models and is in fact quantitatively in line with the ECS values. Grose et al. (2016) scaled CMIP5 projections by ECS values to estimate temperature projections under the full *likely* range of ECS, and if ECS is 6 °C then we may expect a projection of 5.4 to 6.7 °C (using AR5 baseline of 1986-2005 to 2080-2099) with linear scaling, and 6.0 to 8.5 °C using proportional scaling. The new results with ECS values over 5 °C give projections from this baseline of 6.1 to 6.6 °C, suggesting that the scaled results were broadly indicative.

The effect of higher climate sensitivity on the projected change is seen in these results for the end of the century where the signal is strongest, but is less apparent for near-term periods. Under the highest emissions scenario (SSP5-85), and using the AR5 baseline of 1986-2005 and the 10-90th percentile of the model range for direct comparison with the existing Australian national projections (CSIRO and Bureau of Meteorology 2015), we see the range of change is not significantly different to 2020-2039 (0.7 to 1.4 °C in both), or by 2040-2059 (1.4 to 2.4 °C in CMIP5, 1.6 to 2.8 °C in CMIP6). After mid-century, the two ensembles are significantly different (using a 2-tailed Student's T-test) under SSP5-85/RCP8.5, especially at the top end, for both 2060-2079 (2.2 to 3.7 °C in CMIP5, 2.1 to 4.6 °C in CMIP6) and 2080-2099 (2.8 to 5.1 °C in CMIP5, 3.5 to 6.5 °C in CMIP6). The timing of the temperature rise appears to be consistent with a previous finding that while there is a group of models with high ECS, their transient climate response (TCR) measure of climate sensitivity, defined as the global mean temperature change for a doubling of CO2 in a 1% per year increasing CO_2 experiment, has not increased by as large a margin as the ECS (Meehl et al 2019). The different change to TCR compared to ECS suggested that high sensitivity is expressed as higher temperatures mainly at longer timescales. Using the 1850-1900 baseline as an approximation for the pre-industrial climate, some models within CMIP6 project changes in global and Australian temperature of over 7 °C before the end of the century, which is unprecedented in CMIP5.

There are different rates of 20-year warming in the two ensembles from around mid-century for both the globe and Australia, with rates of warming for Australia exceeding 0.8 °C/decade in some models (Supp. Figure 6). There are also some different 20-year trends in earlier periods, especially at the global scale that are likely related to different historical forcing and different model responses to this forcing in CMIP6 and need further investigation.

4b. Rainfall

Projected change in rainfall during Austral summer and autumn (DJFMAM) is broadly similar in CMIP5 and CMIP6 (Figure 9), with a few notable differences. Unlike CMIP5, the range of change from these 16 CMIP6 models does not include models with a large decrease in rainfall in northern Australia (Figure 9d). In Austral winter and spring (JJASON), CMIP6 supports the broad pattern of rainfall change produced in CMIP5, with greater model agreement (so far) for rainfall increase in western Tasmania and decrease down the entire eastern seaboard (Figure 10). There are two cases where the projection may be more constrained than CMIP5 depending on further models: Southern rainfall in JJASON, and Northern rainfall in DJFMAM. There are other cases where the range already appears wider than CMIP5 at either end of

the distribution (or both): notably in Rangelands and Eastern Australia. Projections for three-month seasons (DJF, MAM, JJA, SON, Supp. Figure 7) show a further breakdown of the seasonal signature in rainfall change and feature broader areas of model agreement on little change in summer and autumn than is seen in DJFMAM as a whole.

The models with an atmospheric resolution greater than 1.2 °lat/lon compared to those with coarser resolution (Supp. Figure 8) show no enhanced drying on the slopes of the Alps as found in downscaling (Grose et al. 2019) or other features of "realised added value" from CORDEX simulations identified by DiVirgilio et al. (Submitted). This may be because the resolution of CMIP6 models is still notably coarser than CORDEX (~0.5 °) or other downscaling (~5 km and ~10 km) used in these other studies.

4c. Daily extremes

For the precipitation indices there is little difference in projections between CMIP5 and CMIP6 for Australia in terms of spatial pattern and mean difference over land (Figure 11b, d, f). However, for temperature extremes (Figure 11a, c, e) CMIP6 is decidedly warmer than CMIP5 with about 1 °C warmer in the coldest night, 1.4 °C warmer in the warmest day and >30 days more contributing to warm spells on average over land. The warming is most marked in northern Australia in TNn, central Australia in TXx and a general continent-wide warming of WSDI.

In terms of time series and model spread, the temperature indices tend to start off cooler in CMIP6 than CMIP5 but see an acceleration somewhere between 2040-2070 (Supp. Figure 9) such that by the end of the century the projections are warmer in CMIP6 compared to CMIP5 which also ties in with the pattern of change seen in Figure 13. This result should be treated with caution as the current available models used in this analysis appear to be the ones that show higher climate sensitivity and therefore we might be subsampling an ensemble that, by design, is warmer. Time series of precipitation indices (Supp. Figure 9) generally show a more mixed pattern of change. Rx1day for example is wetter throughout CMIP6 compared to CMIP5 while there are slightly fewer days over 10 mm and almost no discernible difference in consecutive dry days. In all cases the spread is smaller in CMIP6 compared to CMIP5 but again this is most likely due to the smaller number of models in the ensemble.

Further details on extremes are considered here based on the 1 yr and 10 yr average recurrence intervals (ARI). Changes in ARI are calculated from a historical period (defined here by 1950 to 1999 for the ARI analysis) to a future period (defined here by 2050 to 2099) using the SSP585 pathway. The 10 yr ARI for tasmax increases by 3.8 °C from 45.0 °C to 48.8 °C on average over Australia, based on the ensemble mean, which is a similar magnitude change to the case for the 1 yr ARI which also increases by 3.8 °C (from 42.8 °C to 46.6 °C). There is some variation between models, with the range of projected increase being from 2.1 °C to 6.3 °C for the 10 yr ARI and also for the 1 yr. The same two models represent these extremes in both cases, with the smaller change for IPSL-CM6A-LR and the larger change for UKESM1-0-LL.

For precipitation, the 10 -year ARI increases by 15.5% on average for the ensemble of CMIP6 GCMs used here (with values for individual models ranging from 4.6% to 30.4%), while the 1-year ARI increases by 9.4% (with values ranging from 4.0% to 15.8%). In contrast to the case for extreme tasmax, the projected changes in extreme precipitation are larger for the rarer events (i.e., the 10 -year ARI values are larger than the 1-year ARI values). A larger magnitude climate change response for the more intense precipitation events has been reported in previous studies for Australia based on CMIP5 data (CSIRO and BoM 2015) with changes in the 20-year ARI of around 20 to 30% and changes in the 1-year ARI of around 10 to 20% (based on RCP8.5 for the 2080-2099 period as compared to the 1986-2005 period). It is also noted that the resolution of current GCMs, including for CMIP6, is too coarse to adequately simulate severe thunderstorms and associated extreme convective rainfall events, such that larger magnitude increases than this may be plausible in some cases particularly for short-duration extremes (e.g., hourly extremes associated with super-Clausius Clapeyron processes, Guerrerio et al. 2018).

4d. ENSO, IOD and SAM

In both CMIP5 and CMIP6 under high emissions (RCP8.5 and SSP5-85), the intensity of simulated ENSO increases relative to their historical counterparts (Supp. Figure 4). The maximum relative increases occur in August, indicating that the ENSO growth rate plays a role in this intensification. The increase is larger in CMIP6 under SSP5-85 than in CMIP5 under RCP8.5, presumably because the tropical Pacific mean-state warming is greater in the former (not shown). These results are consistent with those from previous studies based on CMIP5 models (Cai et al., 2014, 2015), which show an increase in the frequency of (extreme) El Niño and La Niña events under future global warming. However, when the model simulations were individually examined, a substantial number also showed a decrease in ENSO amplitude under strong radiative forcings (Chen et al., 2017; Rashid et al., 2016). Therefore, it will be important to extend the MMM results by looking at simulated ENSO events and their changes under global warming in individual CMIP6 models.

Under high emissions (RCP8.5 and SSP5-85) the location of peak simulated zonal SST variability differs significantly from the historical experiments (Supp. Figure 4 Bottom panel, lower boxplot). The MMM of available simulations shows that the location of the centre of action is displaced further westwards. Peak variability is moved by about 3° longitude based on the MMM of 31 CMIP5 simulations, and 7° longitude based on 19 CMIP6 models. This westward displacement of peak variability is larger for CMIP6 models compared to CMIP5 models.

SAM is projected to become more positive in the future climate under RCP8.5/SSP-585, with similar results in CMIP5 and CMIP6, and all CMIP6 models considered here agreeing on the sign of this trend (Supp Figure 5). Projected trends have a different seasonal signature than past trends featuring a maximum increase in late autumn and winter rather than summer, due to competing influences from ozone depletion and greenhouse gas forcings in that season during the first half of the century. Given the impact of SAM on rainfall variability shown in previous studies (and well reproduced in the historical CMIP5 and CMIP6 runs, not shown), it seems important to diagnose how much of the projected rainfall change over Australia can result from the projected positive SAM trend. Following the methodology in Lim et al (2016), we estimate the change in Australian rainfall that is congruent with the change of SAM by regressing rainfall onto detrended SAM in CMIP6 HIST and scaling for each model this regression coefficient by the change in SAM from 1995-2014 to 2080-2099. Results in Fig? suggest that the positive SAM trend mostly contributes to the drying of midlatitudes in winter (e.g. in particular over Southwest Western Australia and the southeastern tip of the country) while mitigating the drying over Eastern Australia in that season. In summer, there are suggestions that changes in SAM may enhance the projected wetting of Southeastern Australia.

4e. Dynamic Sea level

Both the CMIP5 and CMIP6 ensembles produce similar features of DSL projections over 2080-2099 relative to 1995-2014 (Figure 7), with high sea levels of around 6 to 12 cm off the southeast coast of Australia, extending from ~30 °S to 45 °S (Figure 7d, e). Off the East Coast, there is a strong north-south contrast of DSL changes, with smaller (larger) rise in the north (south). Along and off the Australian south and southwest coasts, there are around 2 to 4 cm negative DSL changes. Along the Australian northwest and north coasts, the DSL changes are relatively weak, close to zero. The contrast between positive DSL changes off East coast and negative DSL changes off south and southwest coasts can be explained by the spin-up of super gyre (Ridgway and Dunn 2007; Zhang et al. 2017). This contrast around Australia is slightly stronger in CMIP6 than in CMIP5 (Figure 7d, e), which could be due to absence of low-resolution models in the CMIP6 ensemble.

Both CMIP5 and CMIP6 models have a typical nominal oceanic resolution of 1 °lat/lon and cannot explicitly resolve meso-scale eddies. In contrast, dynamical downscaling with 1/10 °lat/lon OGCM reveals some detailed regional features, which are absent in the coarse-resolution CMIP5/6 result (Zhang et al. 2017). For instance, there is a narrow meridional band of high sea levels of around 20 to 30 cm immediately off the southeast coast, extending from ~30 °S to 45 °S, which is closely related to the poleward shifting and strengthening of East Australia Current (EAC) under the future climate. The contrast between the east coast and the south coast is also stronger in the downscaled result. Using

downscaled results as a reference, there is some improvement in the CMIP6 DSL projections, but CMIP6 still cannot resolve some finer-scale features around Australia especially in the EAC and its extension region.

5. Conclusions

This paper presents a collection of evaluation and projections information about climate change in Australia from the available CMIP6 ensemble, placed in the context of information from the CMIP5 ensemble. It is important to reiterate here that differences between the two ensembles are due to several factors. Differences between CMIP5 and CMIP6 in their evaluation compared to observations are in part be due to the sophistication of the models, e.g. the proportion of Earth System Models, the representation of aerosol effects, model resolution and parameterisation improvements. Differences in the projections are due in part to issues such as model climate sensitivity to greenhouse gas concentrations, and some contribution from differences in the greenhouse gases and aerosol forcing scenarios (e.g. RCP8.5 and SSP-585 both reach 8.5 Wm-2 enhanced radiative forcing by 2100 but the proportion of different greenhouse gases and aerosol pathways are different). We do not attempt to attribute the ensemble differences to specific processes or mechanisms, instead focusing on reporting the differences across a range of metrics.

We find a number of differences between the two ensembles, highlighted and discussed in detail in the previous sections. Incremental improvements in the historical mean state is found in the CMIP6 ensemble compared to CMIP5, however significant regional biases remain, for example over the Maritime Continent and the western equatorial Pacific. While the range of strength between important teleconnections between regional climate drivers and Australian rainfall is marginally improved (reduced), in general the strength of these teleconnections is too weak. The simulated temperature and rainfall extremes are similar in the two ensembles, with the exception of the projected change in temperature extremes, which is larger in CMIP6, potentially due to increased climate sensitivity. The simulation of marine heatwaves and dynamic sea level is found to be improved, although the projections remain similar between the ensembles.

The projections of Australian mean and extreme climate variables is broadly similar in CMIP5 and CMIP6 in terms of directions of change and spatial distributions. Both ensembles project warming temperatures and increases in hot extremes proportional to the greenhouse forcing, but CMIP6 provides a hotter high end to projections beyond 2050, including a change of over 6 °C mean annual temperature since the pre-industrial era by 2100 under a high emissions scenario. Unless and until this projection can be confidently rejected, it must be accepted as a credible finding. Both CMIP5 and CMIP6 project a significant drying of southwest Australia in the cool season and less certain or less significant rainfall projections elsewhere

In time the full CMIP6 ensemble will become available, however using the available archive we have already shown in the present study some of the apparent improvements as well as some notable similarities between the state-of-the-art model projections compared to the previous generation. This information should inform regionally relevant climate change projections for Australia.

Table 1. CMIP6 models and runs used in this study for each analysis listed by figure number (marked Fig). Also shown is the models' atmospheric spatial resolution, their reported effective climate sensitivity (ECS), temperature projection for Australian temperature between 1995-2014 and 2080-2099 under SSP5-85.

	Model name:	Run used	Fig	Atmos. Lat/lon grid (°)	Ocean Lat/lon grid (°)	ECS (°C)	Aus proj 2090 SSP5-85 (°C)
1	ACCESS-CM2	r1i1p1f1	1-10	1.2 x 1.8	1.0 x 0.7	4.7	5.8
2	ACCESS-ESM-1-5	r1i1p1f1	1-10	1.2 x 1.8	1.0 x 0.7	3.9	4.6
3	AWI	r1i1p1f1	8	0.9 x 0.9			4.1
4	BCC-CSM2-MR	r1i1p1f1	1-11	1.1 x 1.1	1.0 x 0.7	3.1	3.5
5	BCC-ESM1	r1i1p1f1	1-7	2.8 x 2.8	1.0 x 0.7	3.3	
6	CAMS-CSM1-0	r1i1p1f1	1-5,7-10	1.1 x 1.1		2.3	2.7
7	CanESM5	r1i1p1f1	1-10	2.8 x 2.8	1.0 x 0.8	5.6	6.3
8	CESM2	r1i1p1f1	1-10	0.9 x 1.3	1.1 x 0.4	5.2	5.2
9	CESM2-WACCM	r1i1p1f1	1-5,7-10	0.9 x 1.3		4.7	5.8
10	CNRM-CM6-1	r1i1p1f2	1-11	1.4 x 1.4	1.0 x 0.8	4.8	5.8
11	CNRM-ESM2-1	r1i1p1f2	1-11	1.4 x 1.4	1.0 x 0.8	4.8	5.0
12	E3SM-1-0	r1i1p1f1	8	0.7 x 0.7		5.3	5.3
13	EC-Earth3	r2i1p1f1	6	0.7 x 0.7	1.0 x 0.8	4.2	
14	EC-Earth3-Veg	r1i1p1f1	1-10	0.7 x 0.7	1.0 x 0.8	4.3	4.3
15	FGOALS-g3	r1i1p1f1	1-5,7	2.3 x 2.0			
16	GFDL-CM4	r1i1p1f1	1-11	1.0 x 1.3	0.3 x 0.2	3.9	4.0
17	GFDL-ESM4	r1i1p1f1	1-5,7	1.0 x 1.3		2.7	
18	GISS-E2-1-G	r1i1p1f1	1-5,7	2.0 x 2.5		2.4	
19	GISS-E2-1-G-CC	r1i1p1f1	1-5,7	2.0 x 2.5			
20	GISS-E2-1-H	r1i1p1f1	1-5,7	2.0 x 2.5		3.1	
21	HadGEM3-GC3.1	r1i1p1f3	6		1.0 x 0.8	5.5	
22	INM-CM4-8	r1i1p1f1	8	1.5 x 2.0		1.8	3.0
23	INM-CM5-0	r1i1p1f1	8	1.5 x 2.0		1.9	3.1
24	IPSL-CM6A-LR	r1i1p1f1	1-15,7-11	1.3 x 2.5	1.0 x 0.8	4.5	5.2
25	K-ACE	r1i1p1f1				5.1	
26	MCM-UA-1-0	r1i1p1f1	1-5,7	2.2 x 3.8		3.6	
27	MIROC6	r1i1p1f1	1-5,7-10	1.4 x 1.4		2.6	3.4
28	MIROC-ESM2L	r1i1p1f1	1-5,7-10	2.7 x 2.8		2.7	3.3
29	MPI-ESM-1.2	r1i1p1f1		0.9 x 0.9		3.0	
30	MRI-ESM2-0	r1i1p1f1	1-5,7-11	1.1 x 1.1		3.2	4.2
31	NESM3	r1i1p1f1	1-7	1.9 x 1.9	1.0 x 0.8	4.7	
32	NorCPM1	r1i1p1f1	1-5,7	1.9 x 2.5			
33	NorESM2-LM	r1i1p1f1	2	1.9 x 2.5	1.0 x 0.5	2.5	
34	SAM0-UNICON	r1i1p1f1	1-7	0.9 x 1.3	1.1 x 0.4	3.6	
35	UKESM1-0-LL	r1i1p1f2	1-11	1.3 x 1.9	1.0 x 0.8	5.3	6.2

623 **Table 2** CMIP5 models used, details as for Table 1

	Model	Runs used	Fig	Atmos. Lat/lon grid (°)	Ocean Lat/lon grid (°)	ECS (°C)	Aus proj 2090 RCP85 (°C)
1	ACCESS-1.0	r1i1p1	1-11	1.3 x 1.9	1.0 x 0.7	3.8	4.5
2	ACCESS-1.3	r1i1p1	1-10	1.3 x 1.9	1.0 x 0.7		4.6
3	BCC-CSM1-1	r1i1p1	1-11	2.8 x 2.8	1.0 x 0.7		3.2
4	BCC-CSM1-1-m	r1i1p1	1-5,7-11	2.8 x 2.8	1.0 x 0.7		3.1
5	BNU-ESM	r1i1p1	1-11	2.8 x 2.8	1.0 x 0.9		3.9
6	CanESM2	r1i1p1	1-11	2.8 x 2.8	1.4 x 0.9	3.7	4.9
7	CCSM4	r1i1p1	1-11	0.9 x 1.3	1.1 x 0.4		3.5
8	CESM1-BGC	r1i1p1	1-5,8	0.9 x 1.2	1.1 x 0.6		3.6
9	CESM1-CAM5	r1i1p1	1-5,8	0.9 x 1.3	1.1 x 0.6		4.1
10	CESM1-CAM5-1-FV2	r1i1p1	1-5	0.9 x 1.3	1.1 x 0.6		
11	CESM1-FASTCHEM	r1i1p1	1-5	0.9 x 1.3	1.1 x 0.6		
12	CESM1-WACCM	r1i1p1	1-5	1.9 x 2.5	1.1 x 0.6		
13	CMCC-CESM	r1i1p1	1-11	3.4 x 3.8	2.0 x 1.6		
14	CMCC-CM	r1i1p1	1-11	0.7 x 0.8	2.0 x 1.6		4.8
15	CMCC-CMS	r1i1p1	1-11	3.7 x 3.7	2.0 x 1.6		5.1
16	CNRM-CM5	r1i1p1	1-11	1.4 x 1.4	1.0 x 0.8	3.3	3.6
17	CNRM-CM5-2	r1i1p1	1-5	1.4 x 1.4	1.0 x 0.8		
18	CSIRO-Mk3-6-0	r1i1p1	1-11	1.9 x 1.9	1.9 x 1.9	4.1	4.8
19	FIO-ESM	r1i1p1	1-5	2.8 x 2.8	1.1 x 0.6		
20	FGOALS-g2	r1i1p1	1-5,7-11	2.8 x 2.8	1.0 x 1.0		
21	FGOALS-s2	r1i1p1	1-5,7-11	1.7 x 2.8	1.0 x 1.0		
22	GFDL-CM2p1	r1i1p1	1-5	2.5 x 2.0	1.0 x 1.0		
23	GFDL-CM3	r1i1p1	1-11	2.0 x 2.5	1.0 x 0.9	4.0	4.6
24	GFDL-ESM-2G	r1i1p1	1-11	2.0 x 2.0	1.0 x 0.9		2.8
25	GFDL-ESM-2M	r1i1p1	1-11	2.0 x 2.5	1.0 x 0.9		3.6
26	GISS-E2-H	r1i1p1	1-5,8	2.0 x 2.5	1.0 x 1.0		2.8
27	GISS-E2-H-CC	r1i1p1	1-5,8	2.0 x 2.5	1.0 x 1.0		2.7
28	GISS-E2-R	r1i1p1	1-5,8	2.0 x 2.5	1.0 x 1.3		2.7
29	GISS-E2-R-CC	r1i1p1	1-5,8	2.0 x 2.5	1.0 x 1.3		2.6
30	HadCM3	r1i1p1	1-5	3.7 x 2.5	1.2 x 1.2		
31	HadGEM2-AO	r1i1p1	1-5	1.9 x 1.2	1.0 x 1.0		
32	HadGEM2-CC	r1/2i1p1	1-11	1.3 x 1.9	1.0 x 0.8		4.5
33	HadGEM2-ES	r1/2i1p1	1-11	1.3 x 1.9	1.0 x 0.8	4.6	4.8
34	INMCM4	r1i1p1	1-11	1.5 x 2.0	0.7 x 0.4	2.1	3.3
35	IPSL-CM5A-LR	r1i1p1	1-11	1.9 x 3.8	2.0 x 1.6	4.1	4.8
36	IPSL-CM5A-MR	r1i1p1	1-11	1.3 x 2.5	2.0 x 1.6		5.1
37	IPSL-CM5B-LR	r1i1p1	1-11	1.9 x 3.8	2.0 x 1.6		3.5
38	MIROC5	r1i1p1	1-11	1.4 x 1.4	1.7 x 1.3	2.7	2.7
39	MIROC-ESM	r1i1p1	1-11	2.8 x 2.8	1.4 x 0.8	4.7	4.0
40	MIROC-ESM-CHEM	r1i1p1	1-11	2.8 x 2.8	1.4 x 0.8		4.1
41	MPI-ESM-LR	r1i1p1	1-11	1.9 x 1.9	1.4 x 1.3	3.6	4.3
42	MPI-ESM-MR	r1i1p1	1-11	1.9 x 1.9	0.5 x 0.4		4.2
43	MPI-ESM-P	r1i1p1	1-5	1.9 x 1.9	1.5 x 1.5		
44	MRI-CGCM3	r1i1p1	1-11	1.1 x 1.1	1.0 x 0.5	2.6	3.3
45	MRI-ESM	r1i1p1	1-10	1.1 x 1.1	1.0 x 0.5		3.4
46	NorESM1-M	r1i1p1	1-11	1.9 x 2.5	1.1 x 0.4	2.8	2.5
47	NorESM1-ME	r1i1p1	1-5,7-10	1.9 x 2.5	1.1 x 0.4		2.6

624

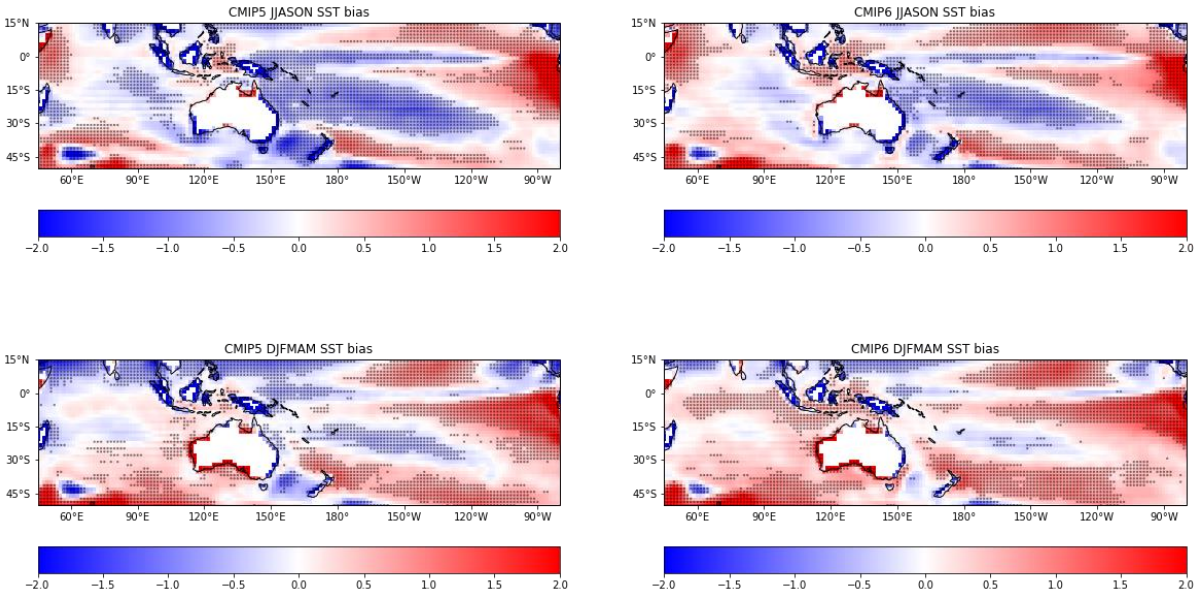

625

626 **Figure 1.** Multi-model sea surface temperature bias (°C) for CMIP5 (left) and CMIP6 (right) models,
627 shown for December to May (DJFMAM, bottom) averages and June to November (JJASON, top)
628 averages. Biases are calculated against the HadISST observation-based dataset for the period 1995-
629 2014. Stipples represent locations where greater than two-thirds of models agree on the sign of the
630 bias.

631

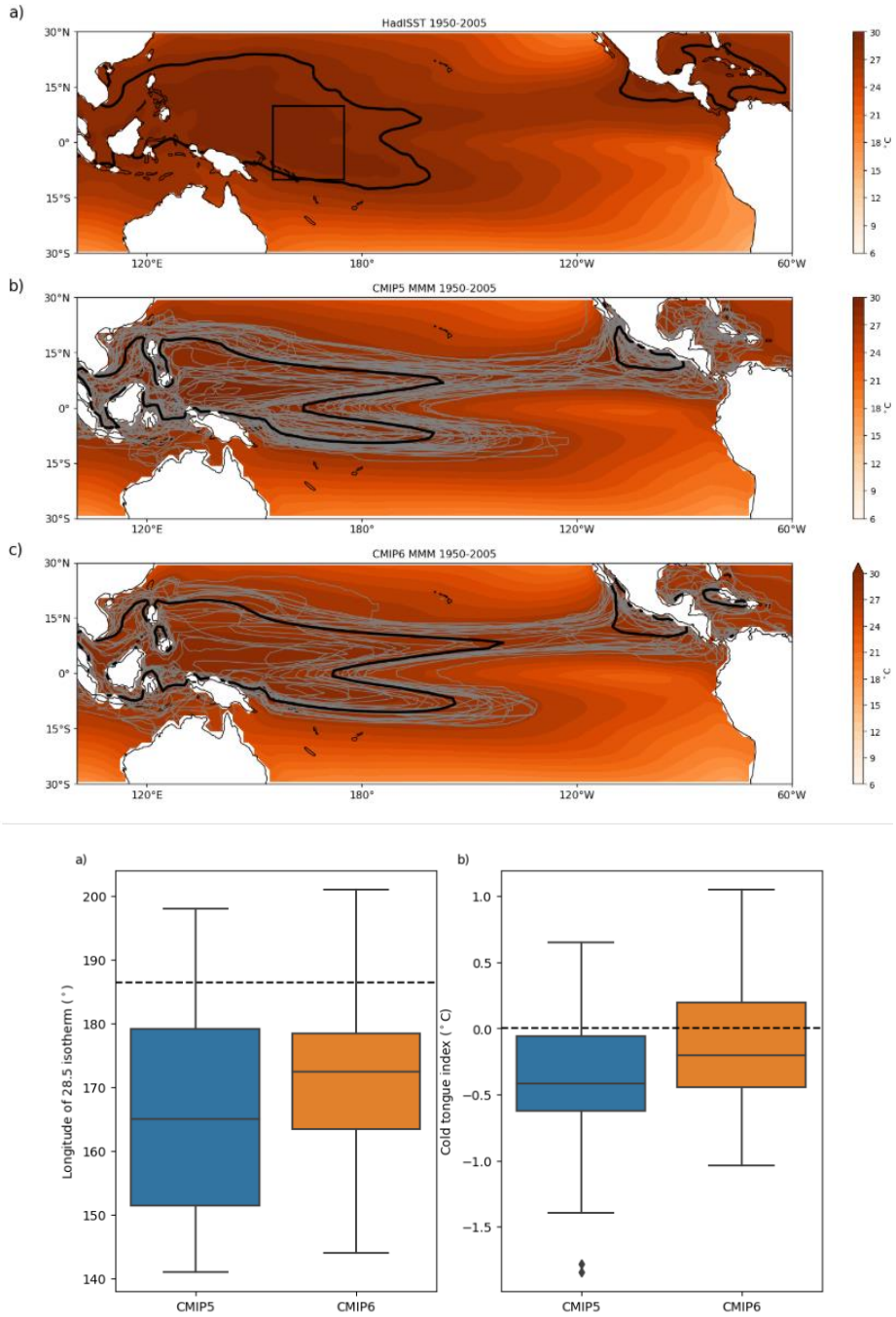

Figure 2. Climatological SSTs from 1950-2005 for JJASON; a) HadISST1.1, the thick black line shows the 28.5 °C isotherm and the box shows the location of the CTI region; b) CMIP5 MMM climatological SSTs for the same period, thin grey lines show the location of the 28.5 °C isotherm for each individual model, and the thick black line shows the MMM; c) the same as b), but for CMIP6; d) box plots of the equatorial longitude of the 28.5°C isotherm for CMIP5 (blue) and CMIP6 (orange), horizontal dashed line shows the observed longitude of the 28.5°C isotherm; e) Box plots of the CTI. In both box plots, the boxes encompass the interquartile range (25%-75% of the model spread) and the whiskers encompass models which lie within 1.5 times the interquartile range of the box borders, outliers are marked as diamonds and the horizontal line in the boxes shows the median.

643

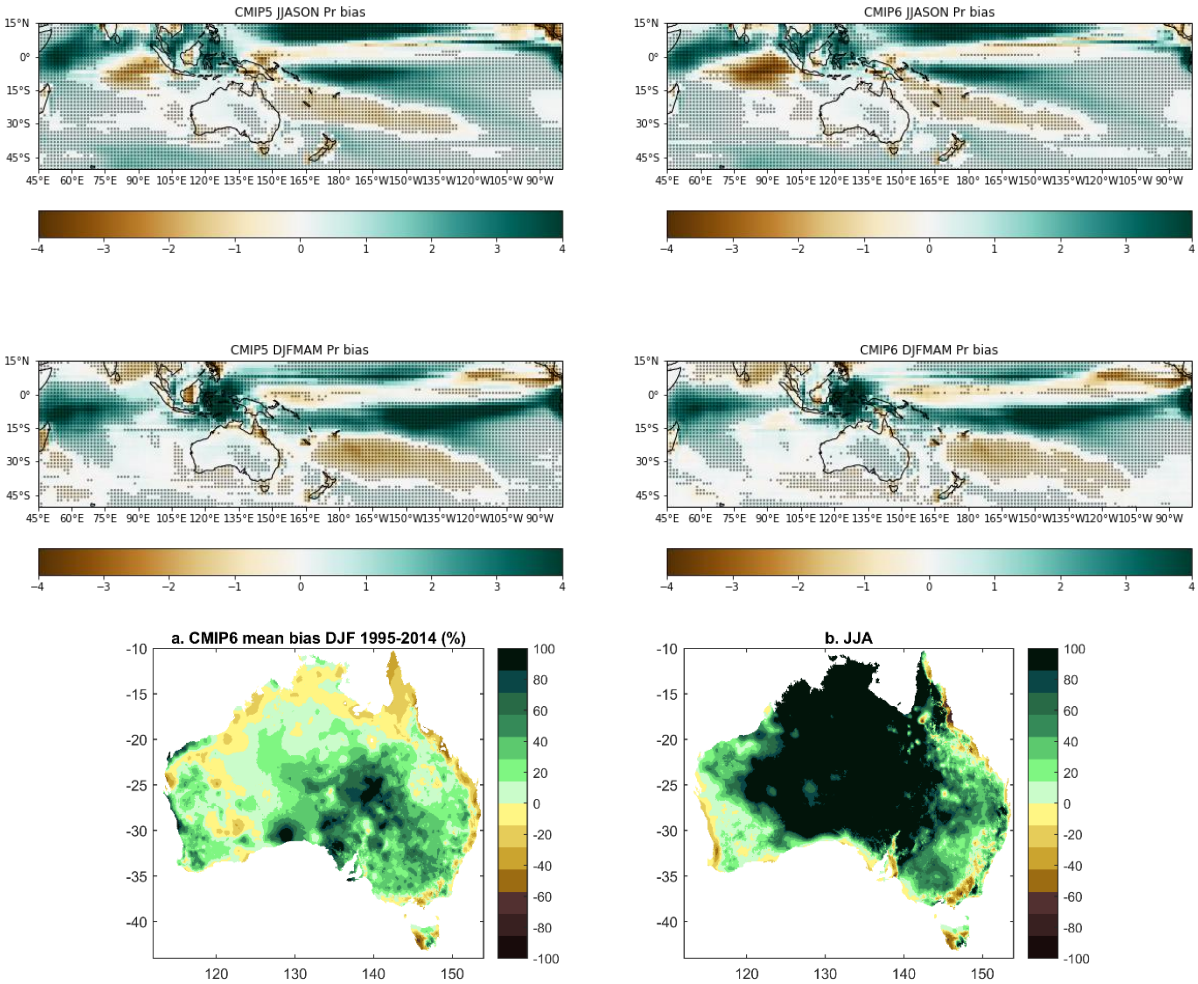

644

645 **Figure 3.** As in Fig 1, except shown for precipitation bias against GPCP observations. Lower panels
646 show mean CMIP6 precipitation bias over Australia in 1995-2014 compared to AWAP, red lines
647 indicate the borders of the four averaging regions used here (coming soon). Stipples represent
648 locations where greater than two-thirds of models agree on the sign of the bias.

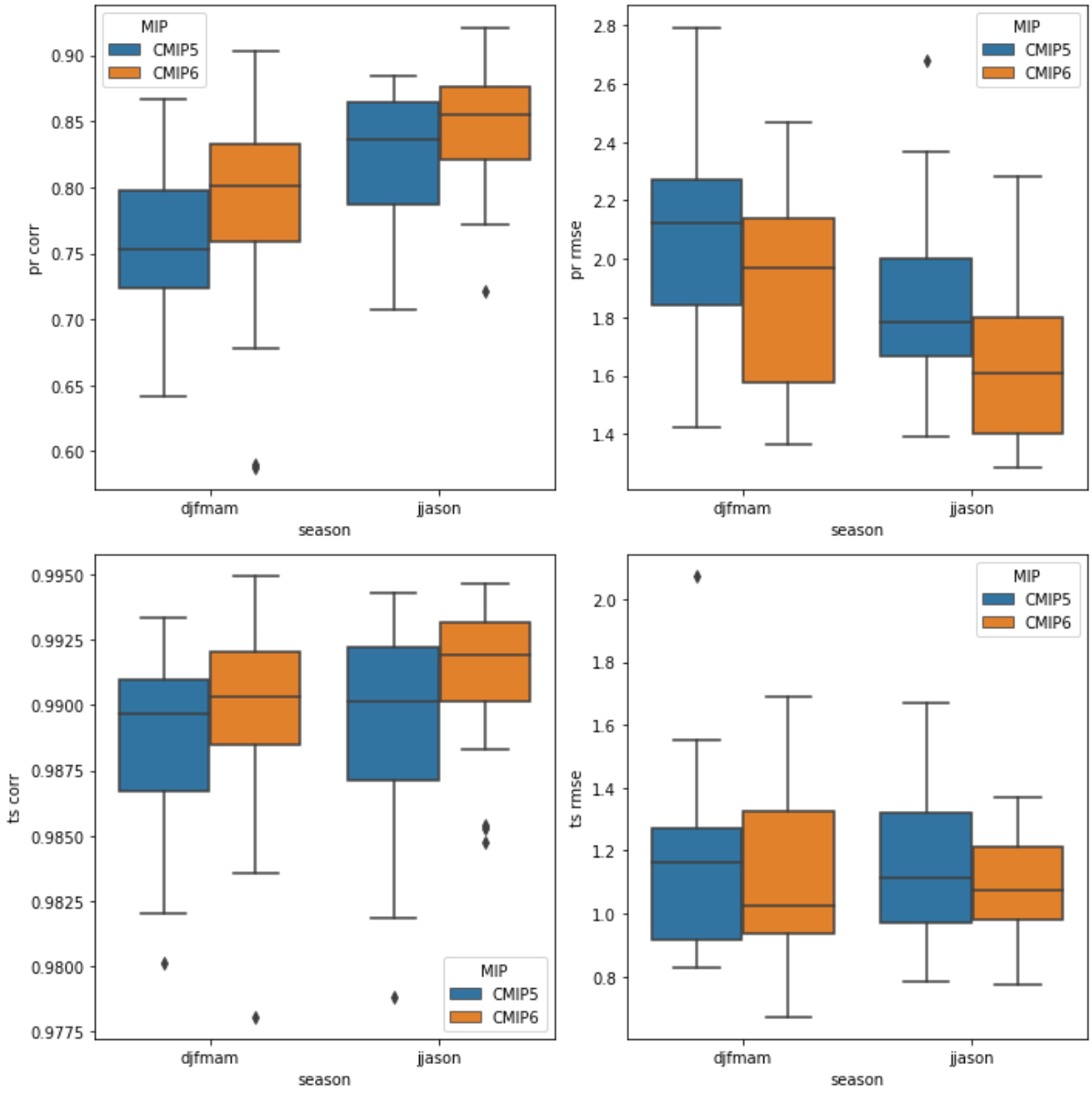

Figure 4. Boxplots of spatial correlation (left) and RMSE (right) for precipitation (top) and surface temperature (bottom) 1996-2014 climatologies, separated by seasons December to May (DJFMAM) and June to November (JJASON), as well as by inter-comparison project (CMIP5 in blue, and CMIP6 in orange). Metrics are calculated for the region 45 to 280 °E, 10 °N to 50 °S. Observational data from GPCP for precipitation and HadISST for SST.

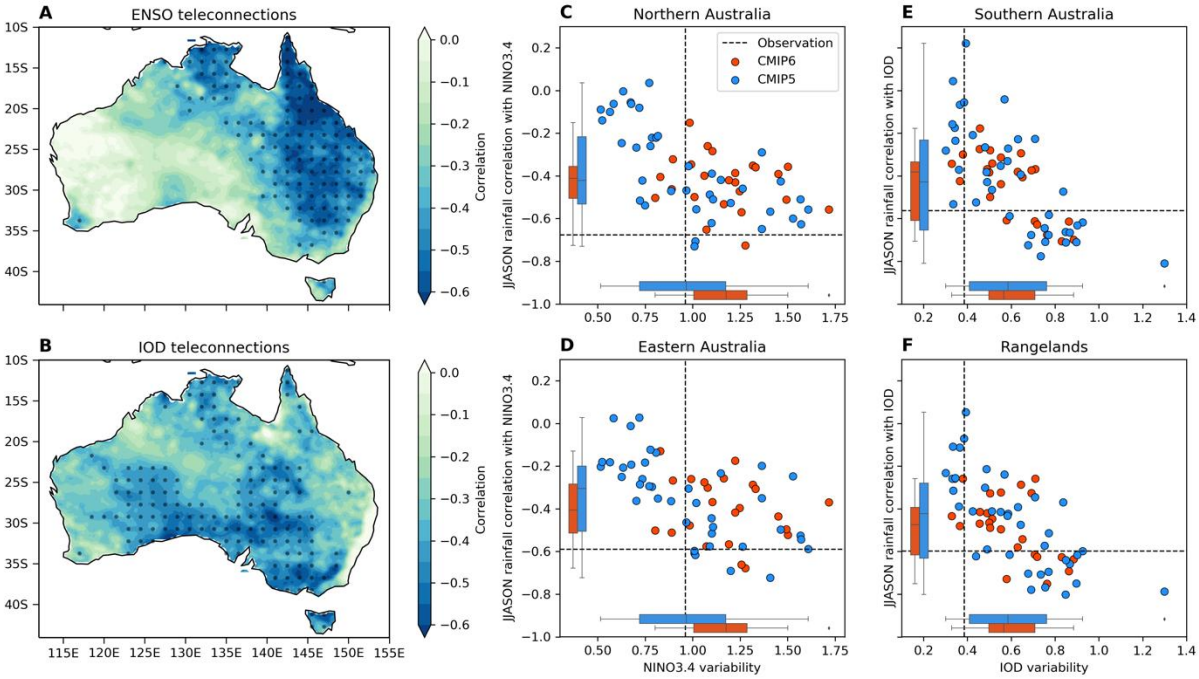

Figure 5. An assessment of the ability of models to simulate ENSO and IOD teleconnections to Australian rainfall. The maps (A, B) show observed correlation coefficients between AWAP winter-spring rainfall and SST indices representing the El Niño Southern Oscillation (A; Niño-3.4) or the Indian Ocean Dipole (B, DMI) in SON. Stippling indicates the 99% significance of the p-value. (C, D, E, F) Scatter plots for the four NRM super clusters, Northern Australia (C), Eastern Australia (D), Southern Australia (E) and the Rangelands (F) showing the correlation coefficient of the cluster-averaged rainfall with the index (Niño-3.4 or the DMI) on the y-axes against the standard deviation of the index which is given on the x-axis. Values for observations (dashed lines), CMIP6 models (orange circles) and CMIP5 models (blue circles) are shown. The boxes show the interquartile model ranges of the x and y axis variables for the CMIP5 (blue) and CMIP6 (orange) models. The whiskers show the rest of the distribution, except for points that are determined to be “outliers" (seaborn boxplot).

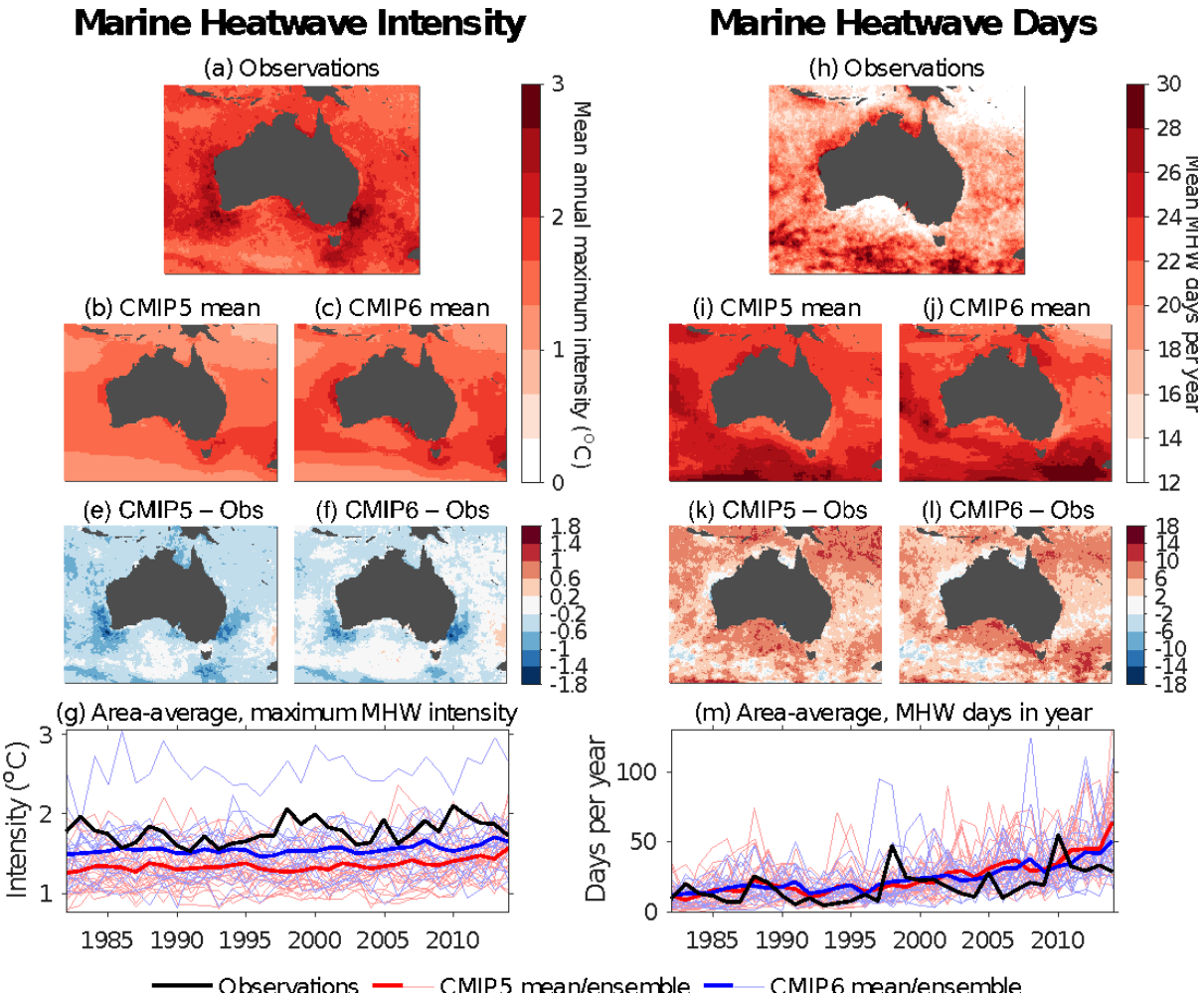

Figure 6. Marine heatwave (MHW) characteristics in observations, CMIP5, and CMIP6 over the period 1982-2014 around Australia. (a) Observed time-mean of the annual maximum MHW intensity. The maximum intensity, relative to the climatology of the base-line period of 1996-2014, is first computed for each calendar year, and each grid-point (see Methods). This panel is thus the mean of each year's maximum intensity. (b,c) As in (a), but for the mean of the CMIP5 and CMIP6 models. (e,f) The difference between (b,c) and (a), representing the model mean biases in MHW intensity. (g) The area-average of maximum MHW intensity over the region depicted in (a-f) shown as annual time-series for the observations, individual CMIP5 and CMIP6 model realisations, and the model means. (h) Observed time-mean of the number of MHW days occurring each year. (i,j) As in (h), but for the mean of the CMIP5 and CMIP6 models. (k,l) The difference between (i,j) and (h), representing the model mean biases in annual MHW days. (m) As in (g), but for the annual MHW days.

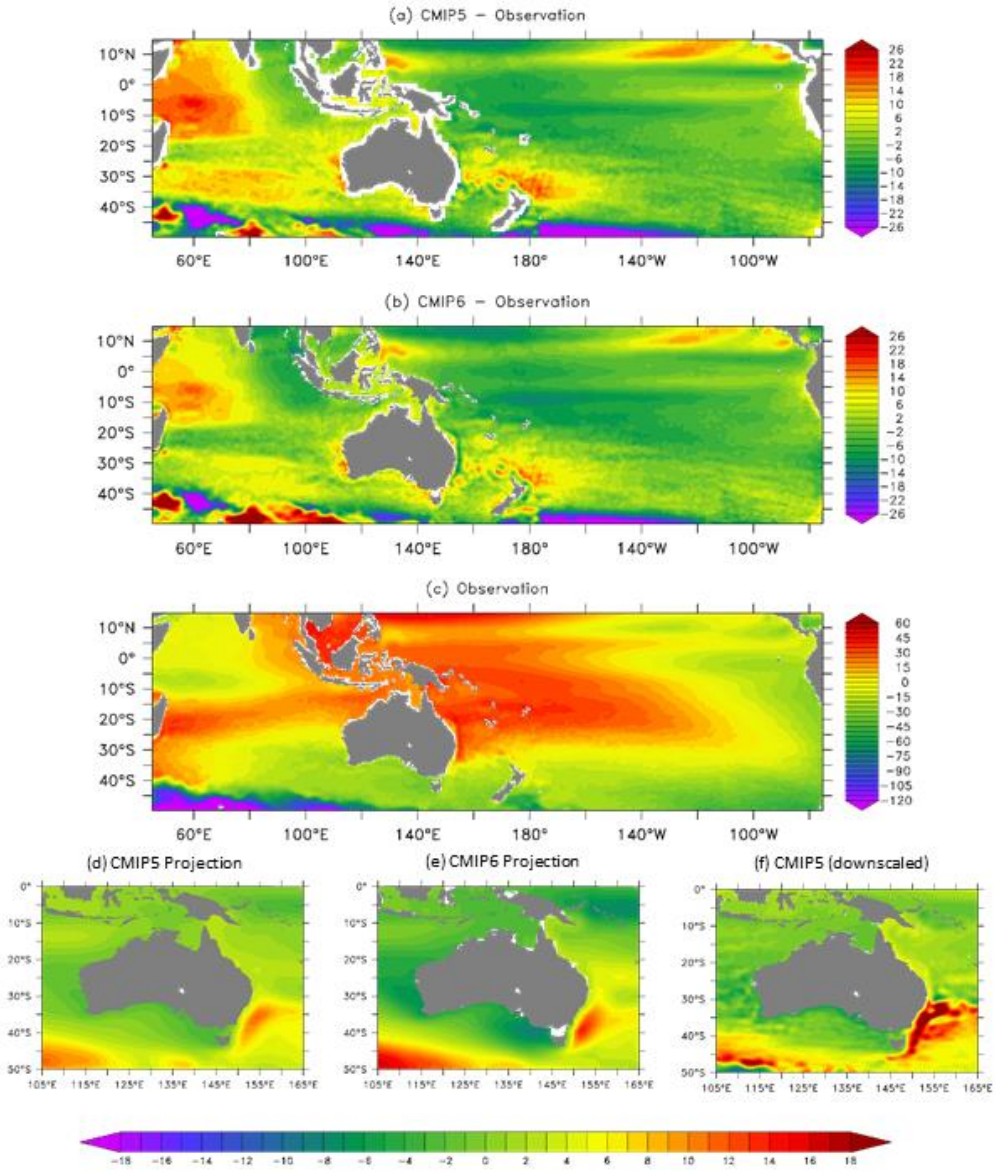

Figure 7. Mean sea level and dynamic sea level projection; a) the CMIP5 MMM difference to observations (in cm) ; b) CMIP6 MMM difference; c) observations (Maximenko et al. 2009). Regional means over (95 to 290 ◦E, 0 to 45◦S) have been removed from both CMIP5/6 ensembles and observations before calculating the differences in (a) and (b). Lower panels show dynamic sea level projections (cm) due to ocean density and circulation change for the Australian region over 2080-2099 relative to 1995-2014 under RCP8.5 from: d) the CMIP5 ensemble; e) CMIP6 ensemble; and f) dynamically-downscaled CMIP5 ensemble.

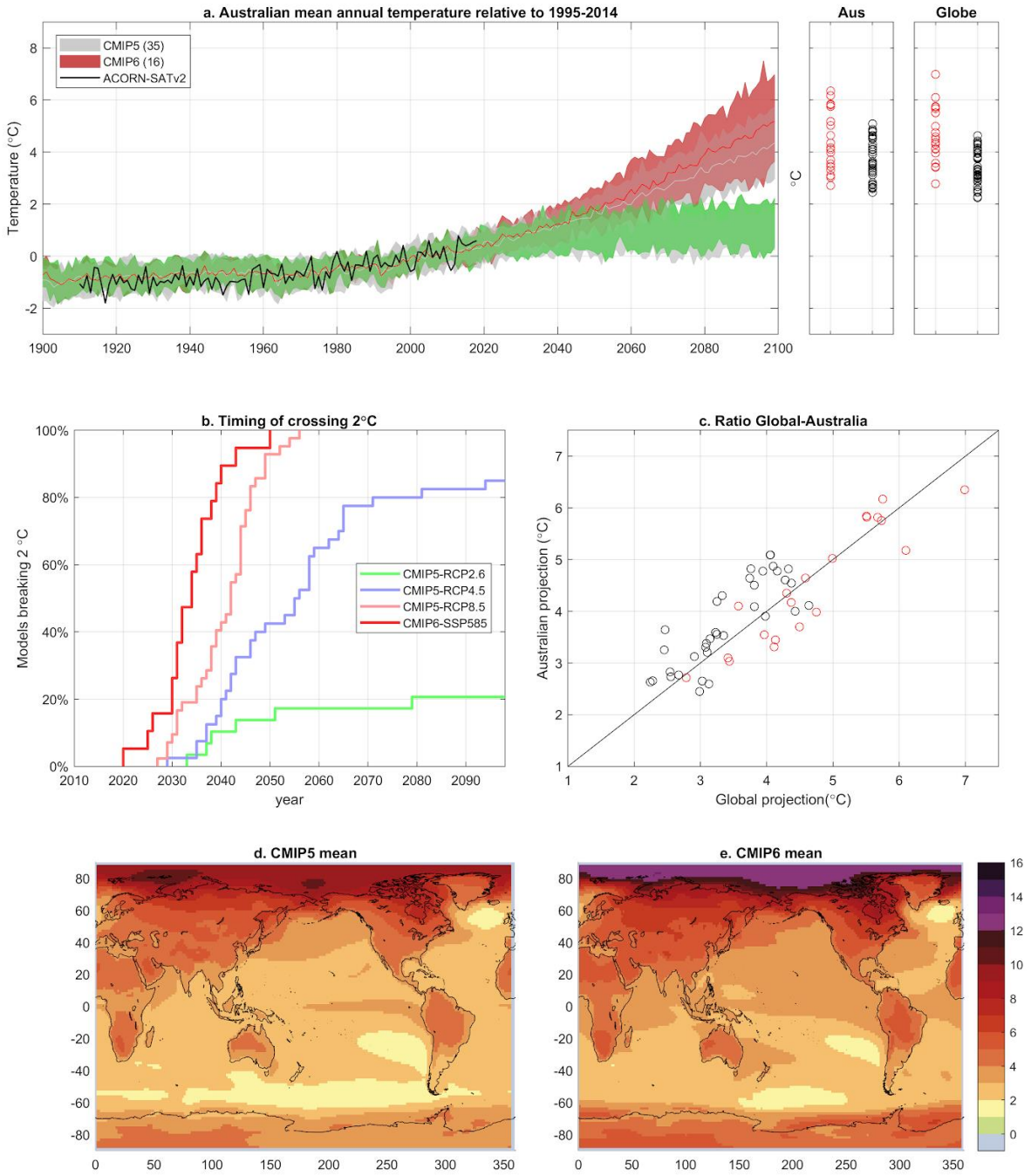

Figure 8. Mean surface air temperature in twenty CMIP6 models and thirty five CMIP5 models for RCP8.5/SSP5-85 except for RP2.6/SSP-126 also shown in panel (a); a) Australian mean anomaly from 1995-2014 average showing 10-90 percentile of model range and the MMM, panels to the right show the value for individual models in 2080-2099 (red is CMIP6, black is CMIP5), b) timing of when model simulations cross 2 °C global warming since pre-industrial times calibrated to the 1986-2005 period (methods taken from Schurer et al. 2018), c) ratio of global to Australian warming at 2080-2099 (red is CMIP6, black is CMIP5), d) multi-model mean warming between 1995-2014 to 2080-2099 in CMIP5, e) as for (d) but in CMIP6.

699

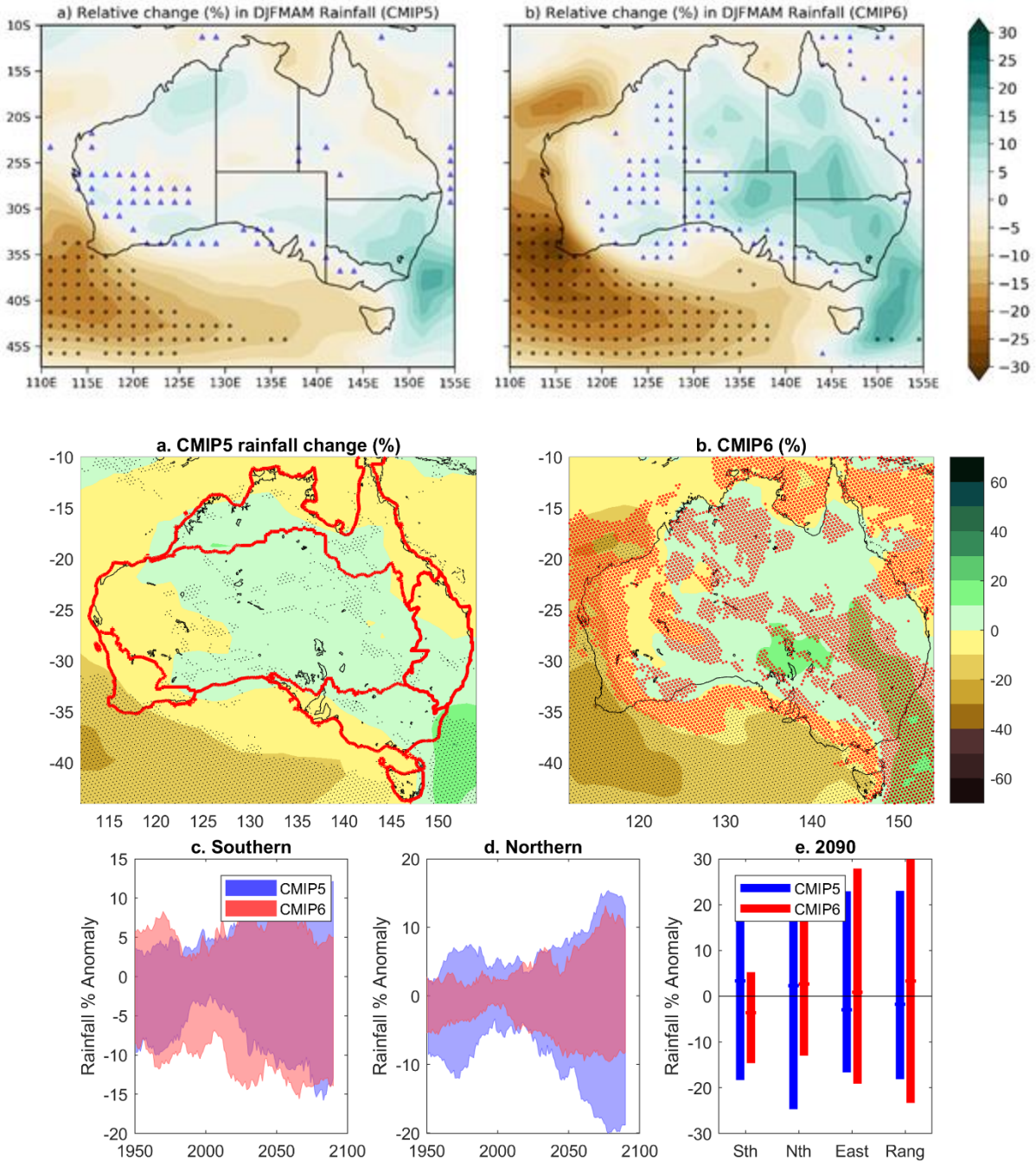

700

701 **Figure 9.** Rainfall projection (%) for summer-autumn (DJFMAM) for 1995-2014 to 2080-2099 under
702 high emissions (RCP8.5 and SSP-585); a) CMIP5 multi-model mean (MMM), stippling shows >90%
703 model agreement on sign of change and blue triangles show regions of small change where the MMM
704 change is less than 0.2 times the MMM standard deviation and less than 20% of models show
705 magnitude of change greater than 2 times the model standard deviation; b) CMIP6 MMM; c) time
706 series of the 10-90% range of CMIP5 and CMIP6 averaged over the Southern region; d) as for (c) but
707 the northern region, and e) range of change in 2080-2099 for each of the four regions (10-90% range,
708 median also indicated).

709

710

711

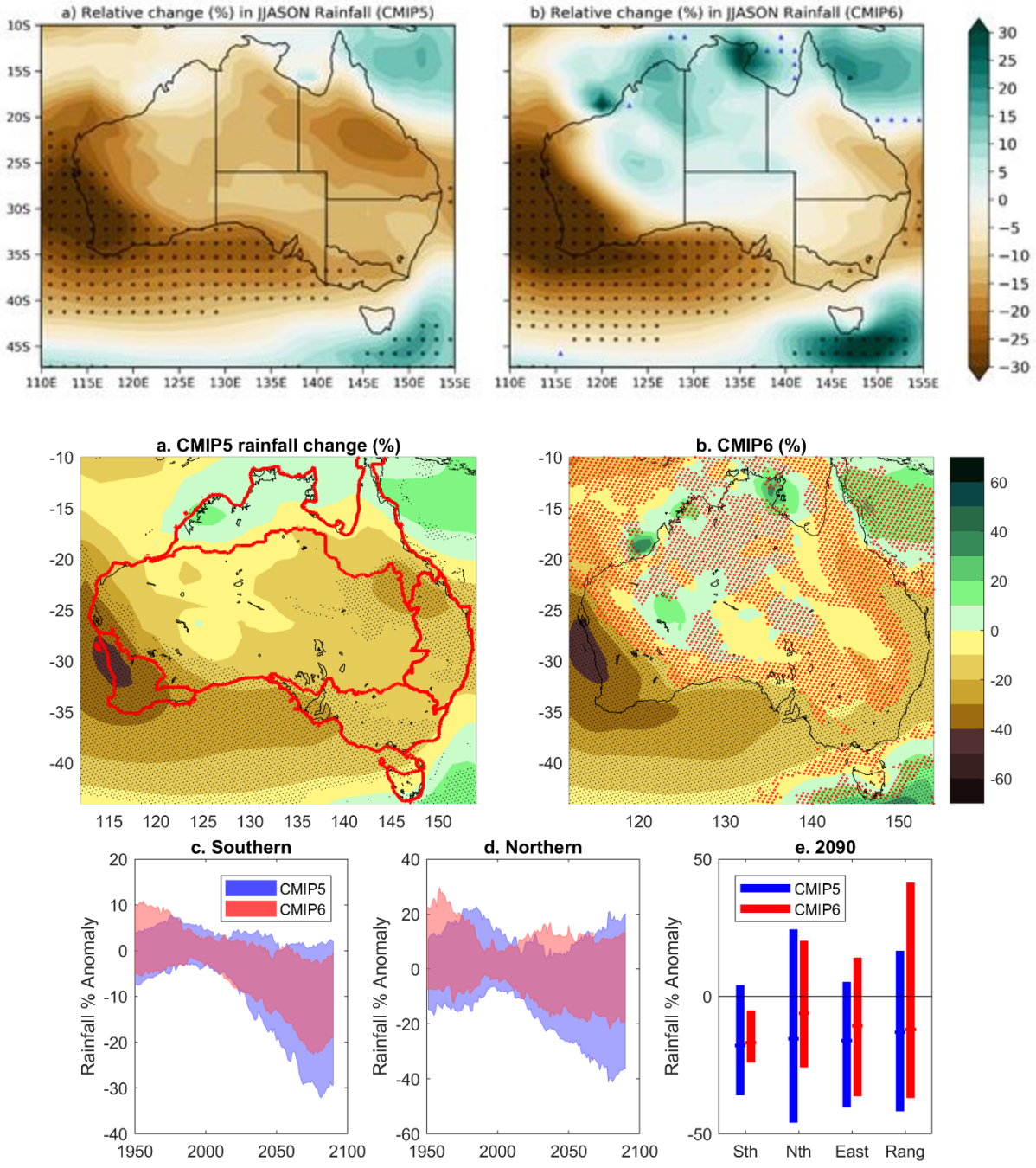

712

713 **Figure 10.** Rainfall projection as for Figure 11 but for winter-spring (JJASON),

714

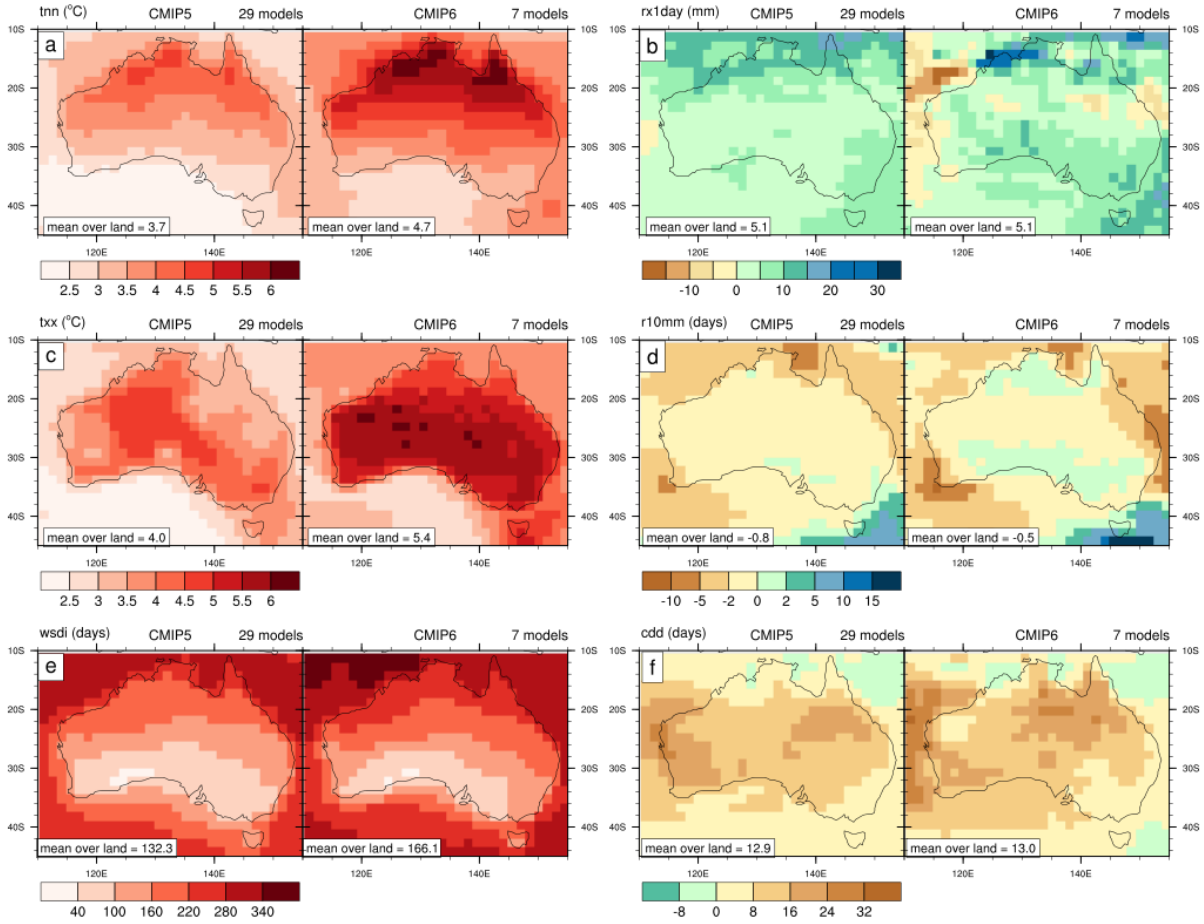

Figure 11. Future change (2080-2099 - 1995-2014) for each of the 6 indices (defined in methods) of temperature (left) and precipitation (right) extremes: (a) tnn, (b) rx1day, (c) txx, (d) r10mm, (e) wsdi, (f) cdd. Each panel compares the CMIP5 (LHS) and CMIP6 (RHS) future change. Number in bottom left corners (very small) indicate the Australia land average of the change. The number of models considered in each ensemble is indicated at the top of the panels.

Acknowledgements

We acknowledge the World Climate Research Programme's Working Group on Coupled Modelling, which is responsible for CMIP, and we thank the climate modelling groups for producing and making available their model output. CMIP5 and CMIP6 model outputs were made available with the assistance of resources from the National Computational Infrastructure (NCI), which is supported by the Australian Government. NOAA High Resolution SST data provided by the NOAA/OAR/ESRL PSD, Boulder, Colorado, USA, from their website at https://www.esrl.noaa.gov/psd/. We acknowledge the support of Australian Government's National Environmental Science Programme's Earth Systems and Climate Change Hub. We thank Martin Dix from CSIRO for calculating ECS indices.

References:

Adler, R.F. and co-authors (2003). The Version-2 Global Precipitation Climatology Project (GPCP) Monthly Precipitation Analysis (1979–Present). *Journal of Hydrometeorology* 4: 1147-1167.

Bellenger, H., Guilyardi, E., Leloup, J., Lengaigne, M. and Vialard, J. (2014). ENSO representation in climate models: from CMIP3 to CMIP5. *Climate Dynamics* 42: 1999-2018.

Brown, J., Moise, A. and Colman, R. (2013a). The South Pacific Convergence Zone in CMIP5 simulations of historical and future climate. *Climate Dynamics* 41: 2179-2197.

Brown, J.N., Langlais, C. and Sen Gupta, A. (2015). Projected sea surface temperature changes in the equatorial Pacific relative to the Warm Pool edge. *Deep Sea Research Part II: Topical Studies in Oceanography* 113: 47-58.

Brown, J.N., Maes, C., Sen Gupta, A., Matear, R.J., Cravatte, S., Langlais, C. and participants, O.w. (2013b). Reinvigorating Research on the Western Pacific Warm Pool – First Workshop. *CLIVAR exchanges* 10.1007/s10584-012-0603-5.

Brown, J.R., Moise, A.F., Colman, R. and Zhang, H. (2016). Will a Warmer World Mean a Wetter or Drier Australian Monsoon? *Journal of Climate* 29: 4577-4596.

Cai, W. and Cowan, T. (2013). Why is the amplitude of the Indian Ocean Dipole overly large in CMIP3 and CMIP5 climate models? *Geophysical Research Letters* 40: 1200-1205.

Cai, W., Sullivan, A. and Cowan, T. (2009). Rainfall Teleconnections with Indo-Pacific Variability in the WCRP CMIP3 Models. *Journal of Climate* 22: 5046-5071.

Cai, W., van Rensch, P., Cowan, T. and Hendon, H.H. (2011). Teleconnection Pathways of ENSO and the IOD and the Mechanisms for Impacts on Australian Rainfall. *Journal of Climate* 24: 3910-3923.

Christensen, J.H. and co-authors (2013). Climate Phenomena and their Relevance for Future Regional Climate Change. *Climate Change 2013: The Physical Science Basis. Contribution of Working Group I to the Fifth Assessment Report of the Intergovernmental Panel on Climate Change*. T. F. Stocker, D. Qin, G.-K. Plattner et al. Cambridge, United Kingdom and New York, NY, USA, Cambridge University Press 10.1017/CBO9781107415324.028**:** 1217–1308.

Collins, M. and co-authors (2013). Long-term Climate Change: Projections, Commitments and Irreversibility. *Climate Change 2013: The Physical Science Basis. Contribution of Working Group I to the Fifth Assessment Report of the Intergovernmental Panel on Climate Change*. T. F. Stocker, D. Qin, G.-K. Plattner et al. Cambridge, United Kingdom and New York, NY, USA, Cambridge University Press 10.1017/CBO9781107415324.024**:** 1029–1136.

Colman, R.A., Moise, A.F. and Hanson, L.I. (2011). Tropical Australian climate and the Australian monsoon as simulated by 23 CMIP3 models. *Journal of Geophysical Research: Atmospheres* 116.

CSIRO and Bureau of Meteorology (2007). Climate Change in Australia. *Technical Report*. Australia. www.climatechangeinaustralia.gov.au.

CSIRO and Bureau of Meteorology (2015). Climate Change in Australia, Technical Report. Melbourne Australia. www.climatechangeinaustralia.gov.au.

Eyring, V., Bony, S., Meehl, G.A., Senior, C.A., Stevens, B., Stouffer, R.J. and Taylor, K.E. (2016). Overview of the Coupled Model Intercomparison Project Phase 6 (CMIP6) experimental design and organization. *Geosci. Model Dev.* 9: 1937-1958.

Flato, G. and co-authors (2013). Evaluation of Climate Models. *Climate Change 2013: The Physical Science Basis. Contribution of Working Group I to the Fifth Assessment Report of the Intergovernmental Panel on Climate Change*. T. F. Stocker, D. Qin, G.-K. Plattner et al. Cambridge, United Kingdom and New York, NY, USA, Cambridge University Press 10.1017/CBO9781107415324.020**:** 741–866.

Gettelman, A. and co-authors (2019). High Climate Sensitivity in the Community Earth System Model Version 2 (CESM2). *Geophysical Research Letters* 46, 8329– 8337. https://doi.org/10.1029/2019GL083978

Gregory, J.M., Andrews, T., Ceppi, P., Mauritsen, T. and Webb, M.J. (2019). How accurately can the climate sensitivity to CO2 be estimated from historical climate change? *Climate Dynamics* 10.1007/s00382-019-04991-y.

784 Gregory, J.M. and co-authors (2004). A new method for diagnosing radiative forcing and climate
785 sensitivity. *Geophysical Research Letters* 31: n/a-n/a.
786 Grose, M.R. and co-authors (2014). Assessment of the CMIP5 global climate model simulations of the
787 western tropical Pacific climate system and comparison to CMIP3. *International Journal of*
788 *Climatology* 34: 3382-3399.
789 Grose, M.R., Colman, R., Bhend, J. and Moise, A.F. (2016). Limits to global and Australian temperature
790 change this century based on expert judgment of climate sensitivity. *Climate Dynamics*
791 10.1007/s00382-016-3269-2: 1-15.
792 Grose, M.R., Syktus, J., Thatcher, M., Evans, J.P., Ji, F., Rafter, T. and Remenyi, T. (2019). The role of
793 topography on projected rainfall change in mid-latitude mountain regions. *Climate Dynamics*
794 10.1007/s00382-019-04736-x.
795 Guerreiro, S.B., Fowler, H.J., Barbero, R., Westra, S., Lenderink, G., Blenkinsop, S., Lewis, E.
796 and Li, X.F. (2018). Detection of continental-scale intensification of hourly rainfall
797 extremes. *Nature Climate Change 8*(9): 803-807, doi:10.1038/s41558-018-0245-3.
798 Hendon, H. H., D. W. J. Thompson, and M. C. Wheeler (2007). Australian rainfall and surface
799 temperature variations associated with the Southern Hemisphere annular mode. *Journal*
800 *of Climate* 20: 2452–2467.
801 Hendon, H. H., E.-P. Lim, and H. Ngyuen (2014a). Variations of subtropical precipitation and
802 circulation associated with the Southern Annular Mode. *Journal of Climate* 27: 3446–
803 3460.
804 Hobday, A.J. and co-authors (2016). A hierarchical approach to defining marine heatwaves. *Progress in*
805 *Oceanography* 141: 227-238.
806 Holbrook, N.J. and Johnson, J.E. (2014). Climate change impacts and adaptation of commercial marine
807 fisheries in Australia: a review of the science. *Climatic Change* 124: 703-715.
808 Huang, P., Xie, S.-P., Hu, K., Huang, G. and Huang, R. (2013). Patterns of the seasonal response of tropical
809 rainfall to global warming. *Nature Geoscience* 6: 357-361.
810 IPCC (2007). *Contribution of Working Group I to the Fourth Assessment Report of the Intergovernmental*
811 *Panel on Climate Change, 2007.* Cambridge, United Kingdom and New York, NY, USA., Cambridge
812 University Press.
813 IPCC (2013). Climate Change 2013: The Physical Science Basis. *Contribution of Working Group I to the*
814 *Fifth Assessment Report of the Intergovernmental Panel on Climate Change*. T. F. Stocker, D. Qin,
815 G.-K. Plattner et al. Cambridge, UK, and New York, NY, USA, Cambridge University Press.
816 Johnson, J.E. and Holbrook, N.J. (2014). Adaptation of Australia's Marine Ecosystems to Climate Change:
817 Using Science to Inform Conservation Management. *International Journal of Ecology* 2014: 12.
818 Lee, T., Waliser, D.E., Li, J.-L.F., Landerer, F.W. and Gierach, M.M. (2013). Evaluation of CMIP3 and CMIP5
819 Wind Stress Climatology Using Satellite Measurements and Atmospheric Reanalysis Products.
820 *Journal of Climate* 26: 5810-5826.
821 Li, G. and co-authors (2019). Effect of excessive equatorial Pacific cold tongue bias on the El Niño-
822 Northwest Pacific summer monsoon relationship in CMIP5 multi-model ensemble. *Climate*
823 *Dynamics* 52: 6195-6212.
824 Li, G. and Xie, S.-P. (2014). Tropical Biases in CMIP5 Multimodel Ensemble: The Excessive Equatorial
825 Pacific Cold Tongue and Double ITCZ Problems. *Journal of Climate* 27: 1765-1780.
826 Li, G., Xie, S.-P., Du, Y. and Luo, Y. (2016). Effects of excessive equatorial cold tongue bias on the
827 projections of tropical Pacific climate change. Part I: the warming pattern in CMIP5 multi-model
828 ensemble. *Climate Dynamics* 47: 3817-3831.
829 Lim, E.-P., and co-authors (2016). The impact of the Southern Annular Mode on future changes in
830 Southern Hemisphere rainfall, Geophysical Research Letters 43: 7160–7167.
831
832 Liu, L., Xie, S.-P., Zheng, X.-T., Li, T., Du, Y., Huang, G. and Yu, W.-D. (2014). Indian Ocean variability in the
833 CMIP5 multi-model ensemble: the zonal dipole mode. *Climate Dynamics* 43: 1715-1730.
834 Maximenko, N., Niiler, P., Centurioni, L., Rio, M.-H., Melnichenko, O., Chambers, D., Zlotnicki, V. and
835 Galperin, B. (2009). Mean Dynamic Topography of the Ocean Derived from Satellite and Drifting
836 Buoy Data Using Three Different Techniques. *Journal of Atmospheric and Oceanic Technology* 26:
837 1910-1919.

838 Mechoso, C. and co-authors (1995). The Seasonal Cycle over the Tropical Pacific in Coupled Ocean-
839 Atmosphere General Circulation Models. *Monthly Weather Review* 123.
840 Meehl, G. et al. (2019), Context for interpreting equilibrium climate sensitivity and transient climate
841 response from the CMIP6 earth system models, submitted to Science Advances Meinshausen, M.
842 and co-authors (2019). The SSP greenhouse gas concentrations and their extensions to 2500.
843 *Geosci. Model Dev. Discuss.* 2019: 1-77.
844 Meyers, G., McIntosh, P., Pigot, L. and Pook, M. (2007). The Years of El Nino, La Nina, and Interactions
845 with the Tropical Indian Ocean. *Journal of Climate* 20: 2872-2880.
846 NCC-Editorial (2019). The CMIP6 landscape. *Nature Climate Change* 9: 727-727.
847 O'Neill, B.C. and co-authors (2016). The Scenario Model Intercomparison Project (ScenarioMIP) for
848 CMIP6. *Geosci. Model Dev.* 9: 3461-3482.
849 Oliver, E.C.J. and co-authors (2018). Longer and more frequent marine heatwaves over the past century.
850 *Nature Communications* 9: 1324.
851 Oliver E.C.J. and co-authors (2019). Projected Marine Heatwaves in the 21st Century and the Potential for
852 Ecological Impact. *Frontiers in Marine Science* 6: 734.
853 Raupach, M.R., Briggs, P.R., Haverd, V., King, E.A., Paget, M. and Trudinger, C.M. (2009). Australian Water
854 Availability Project (AWAP), final report for Phase 3. *CSIRO Marine and Atmospheric Research*
855 *component*. Canberra, Australia, CSIRO Marine and Atmspheric Research**:** 67 pp.
856 Rayner, N.A., Parker, D.E., Horton, E.B., Folland, C.K., Alexander, L.V., Rowell, D.P., Kent, E.C. and Kaplan,
857 A. (2003). Global analyses of sea surface temperature, sea ice, and night marine air temperature
858 since the late nineteenth century. *Journal of Geophysical Research: Atmospheres* 108: 4407.
859 Reynolds, R.W., Smith, T.M., Liu, C., Chelton, D.B., Casey, K.S. and Schlax, M.G. (2007). Daily High-
860 Resolution-Blended Analyses for Sea Surface Temperature. *Journal of Climate* 20: 5473-5496.
861 Ridgway, K.R. and Dunn, J.R. (2007). Observational evidence for a Southern Hemisphere oceanic
862 supergyre. *Geophysical Research Letters* 34.
863 Risbey, J.S., Pook, M.J., McIntosh, P.C., Wheeler, M.C. and Hendon, H.H. (2009). On the remote drivers of
864 rainfall variability in Australia. *Monthly Weather Review* 137: 3233-3253.
865 Schurer, A.P., Mann, M.E., Hawkins, E., Tett, S.F.B. and Hegerl, G.C. (2017). Importance of the pre-
866 industrial baseline for likelihood of exceeding Paris goals. *Nature Climate Change* 7: 563.
867 Sellar, A.A. and co-authors. (2019). UKESM1: Description and evaluation of the UK Earth System Model.
868 Journal of Advances in Modeling Earth Systems n/a.
869 Smale, D.A. and co-authors (2019). Marine heatwaves threaten global biodiversity and the provision of
870 ecosystem services. *Nature Climate Change* 9: 306-312.
871 Taylor, K.E., Stouffer, R.J. and Meehl, G.A. (2012). An Overview of CMIP5 and the Experiment Design.
872 *Bulletin of the American Meteorological Society* 93: 485-498.
873 Thompson, D. W. J., and J. M. Wallace (2000). Annular modes in the extratropical circulation. Part I:
874 Month-to-month variability. *Journal of Climate* 13: 1000–1016.Toh, Y.Y., Turner, A.G., Johnson,
875 S.J. and Holloway, C.E. (2018). Maritime Continent seasonal climate biases in AMIP experiments
876 of the CMIP5 multimodel ensemble. *Climate Dynamics* 50: 777-800.
877 van Vuuren, D. and co-authors (2011). The representative concentration pathways: an overview. *Climatic*
878 *Change* 109: 5-31.
879 Voosen, P. (2019). New climate models predict a warming surge. Science News.
880 https://doi.org/10.1126/science.aax7217 (2019).
881 Ying, J., Huang, P., Lian, T. and Tan, H. (2019). Understanding the effect of an excessive cold tongue bias
882 on projecting the tropical Pacific SST warming pattern in CMIP5 models. *Climate Dynamics* 52:
883 1805-1818.
884 Zhang X, Alexander L, Hegerl GC, Jones P, Klein Tank A, Peterson TC, Trewin, B, Zwiers FW. 2011. Indices
885 for monitoring changes in extremes based on daily temperature and precipitation data. WIREs
886 Climate Change doi:10.1002/wcc.147

887 Zhang, X., Church, J.A., Monselesan, D. and McInnes, K.L. (2017). Sea level projections for the Australian
888 region in the 21st century. *Geophysical Research Letters* 44: 8481-8491.

889